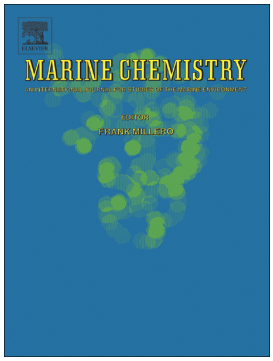

Controls on dissolved and particulate iron distributions in surface waters of the Western Antarctic Peninsula shelf

Amber L. Annett, Jessica N. Fitzsimmons, Marie J.M. Séguret, Maria Lagerström, Michael P. Meredith, Oscar Schofield, Robert M. Sherrell

PII: S0304-4203(16)30157-8
DOI: doi: 10.1016/j.marchem.2017.06.004
Reference: MARCHE 3465

To appear in: *Marine Chemistry*

Received date: 13 October 2016
Revised date: 23 May 2017
Accepted date: 7 June 2017

Please cite this article as: Amber L. Annett, Jessica N. Fitzsimmons, Marie J.M. Séguret, Maria Lagerström, Michael P. Meredith, Oscar Schofield, Robert M. Sherrell , Controls on dissolved and particulate iron distributions in surface waters of the Western Antarctic Peninsula shelf, *Marine Chemistry* (2017), doi: 10.1016/j.marchem.2017.06.004

Controls on dissolved and particulate iron distributions in surface waters of the Western Antarctic Peninsula shelf

Authors:

Amber L. Annett [1]*

Jessica N. Fitzsimmons [1, 2]

Marie J. M. Séguret [1, 3]

Maria Lagerström [1, 4]

Michael P. Meredith [5]

Oscar Schofield [1]

Robert M. Sherrell [1, 6]

[1] Department of Marine and Coastal Sciences, Rutgers University, New Brunswick, USA

[2] Now at: Department of Oceanography, Texas A&M University, College Station, TX, USA

[3] Now at: Department of Earth Sciences, Utrecht University, Utrecht, The Netherlands

[4] Now at: Department of Environmental Science and Analytical Chemistry, Stockholm University, Stockholm, Sweden

[5] British Antarctic Survey, Cambridge UK

[6] Department of Earth and Planetary Sciences, Rutgers University, Piscataway, NJ, USA

***Corresponding author:** Department of Marine and Coastal Sciences, Rutgers University, 71 Dudley Road, New Brunswick, NJ, USA 08901, annett@marine.rutgers.edu

Abstract:

The Western Antarctic Peninsula (WAP) displays high but variable productivity and is also undergoing rapid change. Long-term studies of phytoplankton communities and primary production have suggested transient limitation by the micronutrient iron (Fe), but to date no data have been available to test this hypothesis. Here, we present the first spatially extensive, multi-year measurements of dissolved and particulate trace metals in surface waters to investigate the key sources and sinks of Fe in the central WAP shelf. Surface samples of dissolved and particulate metals were collected throughout the 700 x 200 km grid of the Palmer Long-Term Ecological Research program in three consecutive austral summers (2010-2012).

Iron concentrations varied widely. Both dissolved and particulate Fe were high in coastal waters (up to 8 nmol kg^{-1} and 42 nmol kg^{-1}, respectively). In contrast, very low Fe concentrations (< 0.1 nmol kg^{-1}) were widespread in mid- to outer-shelf surface waters, especially in the northern half of the sampling grid, suggesting possible Fe limitation of primary production on the shelf. Sea ice and dust inputs of Fe were minor, although their relative importance increased with distance from shore due to the larger near-shore sources. Sedimentary inputs were inferred from manganese distributions; these were more significant in the northern portion of the grid, and showed interannual variation in intensity. Overall, the interannual distribution of Fe was most closely correlated to that of meteoric water (glacial melt and precipitation). Although the Fe concentrations and relative contributions of dissolved and particulate Fe attributed to meltwater were variable throughout the sampling region, increasing glacial meltwater flux can be expected to increase the delivery of Fe to surface waters of the coastal WAP in the future.

1. Introduction

The Western Antarctic Peninsula (WAP) is a highly productive, seasonally ice-covered region of the Southern Ocean (Ducklow et al., 2013; Huang et al., 2012; Vernet et al., 2008). During the second half of the twentieth century, the WAP experienced the most dramatic atmospheric winter warming of any region in the southern hemisphere (Bromwich et al., 2012; Hansen et al., 1999). This warming has more recently been compensated (and in places exceeded) by a cooling associated with natural fluctuations in atmospheric circulation (Turner et al. 2016), though there is an expectation that the climatic warming signal will reassert itself at some point in future. Concurrent with the trend of atmospheric warming, the upper-level ocean is also warming (Meredith and King 2005), and duration of seasonal sea ice cover has decreased markedly (Stammerjohn et al., 2012, 2008). Incursions of warm, nutrient-rich Circumpolar Deep Water (CDW) onto the shelf have increased (Martinson and McKee, 2012; Schmidtko et al., 2014), and this deep-ocean warming was determined to be responsible for the retreat of the majority of WAP glaciers (Cook et al., 2016). Ecological responses to these changes have already been observed in phytoplankton dynamics (Montes-Hugo et al., 2009; Moreau et al., 2015) as well as in higher trophic levels (Atkinson et al., 2004; Saba et al., 2014; Steinberg et al., 2015).

In contrast, there has been little investigation of the effects of climate variability and change on the distribution and bioavailability of nutrients, especially the potentially limiting micronutrient iron (Fe). Offshore Antarctic Circumpolar Current (ACC) waters are Fe-limited across much of the Southern Ocean (Boyd et al., 2007; Martin et al., 1990), and mixing with deeper, Fe-replete waters is an important mechanism of Fe supply to surface ACC communities (Holm-Hansen et al., 2005; Tagliabue et al., 2014). The WAP is a key source region of such high-Fe water, and Fe-stimulated primary production has been observed up to 2500 km downstream of the northern WAP in the Scotia Sea (De Jong et al., 2012; Hatta et al., 2013; Klunder et al., 2014). A potential Fe supply mechanism to the WAP shelf euphotic zone is the upwelling of relatively Fe-enriched modified CDW (mCDW), which may acquire Fe as it mixes with shelf water masses and contacts shelf sediments, both on the open WAP shelf (Annett et al., 2015; Bown et al., 2016) and in cavities under ice shelves (Planquette et al., 2013). Sea ice melt (Lannuzel et

al., 2011, 2010), atmospheric dust (Gao et al., 2013; Winton et al., 2015), terrestrial runoff (of precipitation or glacial meltwater) and glacial processes (Annett et al., 2015; Bown et al., 2016) can also be sources of Fe. Glacial sources include sediment delivery from icebergs (Duprat et al., 2016; Lin et al., 2011; Raiswell et al., 2008), direct melting of glacial ice (Gerringa et al., 2012), subglacial meltwater flow (Wadham et al., 2013), and entrainment of glacial Fe into seawater within ice shelf cavities (Gerringa et al., 2012; Planquette et al., 2013, Sherrell et al., 2015).

Although the multiple potential continental input sources suggest high-Fe conditions nearshore, WAP surface waters may not be uniformly replete in Fe as a result of spatially variable inputs and abiotic or biological sinks. Indeed, heterogeneous Fe limitation has been hypothesized previously to explain the distribution of primary production in shelf waters (Garibotti et al., 2003; Huang et al., 2012; Smith et al., 2008). Despite extensive oceanographic survey data from the Palmer Long-Term Ecological Research (Pal-LTER) program (Ducklow et al., 2013; Ross et al., 1996), until recently no trace metal measurements were available from the central WAP shelf with which to assess Fe limitation. The only records from this region are recent time-series studies in Ryder Bay (northern Marguerite Bay), which have established high total dissolvable Fe, significant glacial inputs, deep-water Fe sources, and biological depletion of available Fe (Annett et al., 2015; Bown et al., 2016; Weston et al., 2013). South and west of the WAP, studies in the Pine Island region and Amundsen Sea Polynya have found significant Fe fluxes associated with glacial melting and processes beneath ice shelves (Gerringa et al., 2012; Planquette et al., 2013; Sherrell et al., 2015) and highlighted vertical advection and sea ice inputs in the Bellingshausen Sea (De Jong et al., 2015). Most studies of Fe in the WAP shelf region have focused on Fe distributions near the northern tip of the peninsula and in smaller regions where circulation and bathymetry result in natural Fe fertilization (Scotia and Weddell seas; e.g. Ardelan et al., 2010; De Jong et al., 2012; Dulaiova et al., 2009; Hatta et al., 2013; Hewes et al., 2008; Klunder et al., 2014; Measures et al., 2013; Sañudo-Wilhelmy et al., 2002).

Here we present three consecutive years (2010-2012) of mid-summer surface Fe concentrations, both dissolved and particulate, from the WAP-wide annual sampling of the Pal-LTER grid. To investigate the candidate Fe sources to the shelf ecosystem,

concentrations of particulate aluminum (Al) and titanium (Ti), along with dissolved and particulate manganese (Mn) are also discussed. Like Fe, Al and Ti are both lithogenically derived, but they are not subject to the same biological control. Manganese, like Fe, is released by reductive dissolution from sediments (Froelich et al., 1979; Pakhomova et al., 2007) but is much more soluble than Fe and typically has a longer residence time (Noble et al., 2012).

In the context of ongoing climate change, this study had two goals: (1) characterize the major processes controlling distribution of these elements in WAP surface water, and (2) evaluate the potential impacts of changing supply mechanisms on Fe availability to phytoplankton. A full assessment of the potential for Fe limitation of primary productivity on the WAP shelf and biological uptake of trace metals in this region will be presented elsewhere. The lack of a strong shelf-break front allows CDW incursion and off-shelf transport (Martinson et al., 2008; Moffat et al., 2009), linking WAP shelf processes with offshore and downstream open ocean waters (Jiang et al., 2013b; Zhou et al., 2013). To properly quantify modern and future productivity on the WAP shelf and in this sector of the Southern Ocean, it is clear that an improved understanding of the role of Fe supply and limitation is needed.

2. Methods:

2.1 Study area and oceanographic context

The ongoing Palmer Long Term Ecological Research (Pal-LTER) grid covers a ~700 × 200 km area of the WAP shelf. Sampling lines are arranged perpendicular to the peninsula at 100 km intervals, from the -100 line in the south (Charcot Island) to the 600 line in the north, at the inshore end of which is Palmer Research Station on Anvers Island (Fig. 1). The WAP shelf is broad (~200 km), with complex bathymetry and an average depth of ~450 m. There are several deep enclosed depressions within the Pal-LTER grid: northwest of Alexander Island, northeast of Adelaide Island, and Palmer Deep south of Anvers Island, which has a bottom depth of ~1400 m (Fig. 1). Additionally, several deep glacially-scoured canyons dissect the shelf; Marguerite Trough in particular is a relatively continuous canyon from the shelf break to George VI ice shelf in southern Marguerite Bay, reaching a maximum depth of 1600 m near Alexander Island (Bolmer et al., 2004). These canyons act as conduits for incursions of CDW at depth with eddies also playing a role (Martinson et al., 2008; Martinson and McKee, 2012; Moffat et al., 2009). The proximity of the ACC to the shelf break along the WAP leads to CDW intruding onto the continental shelf in a less modified form than in other Antarctic regions (Klinck, 1998; Meredith et al., 2008), though it is significantly modified by mixing as it transits up the canyons, by cross-canyon ridges and overflow-driven mixing events (Venables et al., 2016)

At depth, most WAP shelf water is mCDW, which is relatively warm and saline with high nutrient concentrations (Martinson et al., 2008; Moffat et al., 2009). Above this is a very cold layer formed by deep winter mixing, termed Winter Water (WW). During winter this extends to the surface, but during summer only a remnant is present as a cold layer at 50-150 m depth. Freshening from melting sea ice, precipitation, and glacial meltwater, and warming from solar insolation combine to form Antarctic Surface Water (AASW) above the WW. Surface currents near the shelf break are dominated by eastward movement of the ACC and recirculation inshore of the ACC (Hofmann and Klinck, 1998). There is also a southwestward flowing Antarctic Peninsula Coastal Current that is at least partially driven by buoyancy forcing from coastal freshwater inputs (Moffat et al., 2008;

Savidge and Amft, 2009), which will likely be affected by accelerating glacial retreat rates (Cook et al., 2016) driven by increasing deep ocean heat content.

2.2 Sample collection and analysis

Samples were collected during the annual Pal-LTER cruises (January) in three successive austral summers (2010-2012) aboard the ARSV *Laurence M. Gould*. Surface water was collected for trace metal analysis using a non-contaminating towfish deployed from a laterally-extended knuckle crane off the starboard side of the ship, avoiding contamination from the ship's hull. Seawater was pumped through an acid-cleaned polyethylene tube (3/8 inch I.D.) using a deck-mounted air-powered double diaphragm pump (Teflon and polypropylene wetted surfaces; Husky model 307, Graco, Inc., Minneapolis, MN, USA). The seaward length of the tube was mated to a 1/2 inch diameter polyester rope, and the paired tube and rope were passed over a plastic-coated sheave suspended from the end of the crane, and attached to a plastic vane with a plastic-coated bronze depressor weight hung 1 m beneath. While towing at speeds up to 11 knots, seawater was collected at ~2 m depth, and pumped into a HEPA-filtered clean lab built within the ship's main science lab, where it was filtered in-line at 0.2 µm through acid-cleaned capsule filters (Acropak 200, Pall®). The only surfaces in contact with seawater in this system were acid-cleaned Teflon, polypropylene, polyethylene, and polyethersulfone. Filtered seawater samples were collected in acid-cleaned low-density polyethylene bottles (Nalgene) and were acidified at sea to pH ~2.0 using ultraclean HCl (Fisher Optima HCl, concentration in seawater 0.012 M) in order to prevent adsorptive loss of metals to container walls and to prevent biological growth.

Meteoric meltwaters from a meltwater stream ~400 m from Palmer Station (Anvers Island) were sampled on 2 February 2015. This small stream is fed by glacial melt but may also have included some proportion of recent snow melt and/or rain, and was flowing over a short area of exposed rock and sediment near the base of the glacier at the time of sampling, before ultimately discharging into Arthur Harbor near Palmer Station. Acid-cleaned, all-polypropylene syringes and 0.45 µm Acrodisk ® filters were rinsed with meltwater, and then 60 mL of filtrate was collected into acid-cleaned low-

density polyethylene bottles following a single bottle rinse. Meltwater was acidified as for seawater.

Seawater and meltwater samples were analyzed at Rutgers University for dissolved Fe and Mn (in addition to Zn, Cu and Ni; to be reported elsewhere) using an automated flow injection ICP-MS method developed in the Sherrell laboratory at Rutgers University (Lagerström et al., 2013). Briefly, the automated device loaded a 9 mL aliquot of seawater, which was buffered inline to pH 7.0 with 3 mL of acetic acid/ammonium hydroxide buffer, onto a column packed with Nobias PA1 chelating resin (Hitachi High-Technologies). The column was rinsed in buffered Milli-Q water and eluted with 1.5 M nitric acid directly into the nebulizer of an Element-1 sector field ICP-MS (Thermo-Finnigan, Bremen, Germany). All acids used for sample analysis were Optima ® grade (Fisher). The eluate, a 200-fold concentrate of the sample with greatly reduced major ion concentrations, was analyzed in medium resolution and temporal peak integration was performed using custom software coded in MATLAB (MathWorks, Newton MA). Quantification for Fe was carried out using isotope dilution (^{57}Fe spike) and for Mn by matrix-matched external standards in seawater, the latter pre-concentrated through the chelating column at the beginning and end of each analytical session, and corrected for instrumental sensitivity drift.

Analytical duplicates were measured every sixth sample and typically displayed 1–3 % deviation about the mean. The long-term precision over many analytical runs over a period of months, as demonstrated by repeated analysis of a large-volume in-house seawater standard from the Ross Sea (analyzed 5–6 times during each analytical session), was 3 % for Fe and Mn (RSD; see Table 3 in Lagerström et al., 2013). Accuracy was verified by repeated analysis of reference seawater materials (SAFe S and D2, GEOTRACES S and D), which showed agreement within one standard deviation of the consensus values for almost all reference seawaters (Table 1).

Methods for the collection and analysis of a suite of major and trace particulate metals including Al, Ti, Fe, and Mn followed Planquette and Sherrell (2012). Briefly, particles were filtered from 1.5 to 8.5 L of towfish-collected whole seawater onto acid-cleaned 0.45 µm pore size filters (47 mm, Supor; Pall®) within the shipboard clean lab. Filters were stored in acid-cleaned PetriSlides ® (Millipore) and immediately frozen for

storage and shipping. At Rutgers, filters were subjected to complete acid digestion in a solution of 8.0 M HNO_3 and 2.9 M HF for 4 hours on a hotplate at ~110 ºC. Elemental composition was quantified by ICP-MS analysis against multi-element external standards, correcting for blank signals from acids, PTFE vials, and filters.

In some samples, low particle concentrations resulted in low absolute particulate metal abundances relative to the blank (≤ twice the mean unused filter blank value). In cases where particulate Fe:Al and Fe:Ti ratios deviated from consistency with the dominant sample range and with trends described by samples from adjacent stations, uncertainty associated with correction for the significant filter blank was deemed to be the cause. For these samples (19% of samples for Fe, 15% for Al, and 12% for Ti) the values were excluded from statistical analysis, although blank-corrected concentrations are displayed on figures as open symbols to show when and where these very low values occurred.

2.3 Supporting data

Salinity and temperature were recorded at each sampling location from the continuous underway monitoring system on the ARSV *Laurence M. Gould* to match the trace metal sampling resolution, and are available through the Pal-LTER DataZoo (http://oceaninformatics.ucsd.edu/datazoo/data/pallter/datasets). Seawater oxygen isotope data ($\delta^{18}O$ of H_2O) have been presented in Meredith et al. (2013, 2016), following the sample collection and analysis described therein. From $\delta^{18}O$ and salinity we have calculated proportions of meteoric water (glacial melt plus precipitation) and sea ice melt relative to the mean properties of WW (winter mixed layer "WML" in Meredith et al. (2013), following their equation 2). All $\delta^{18}O$-derived freshwater fractions are presented here with respect to the mean WW for the Pal-LTER grid.

3. Results

3.1 Oceanographic conditions and meltwater input

Surface waters showed different sea surface temperature (SST) and salinity (SSS) ranges in each of the three sampling years (Fig. 2). In the first two years sampled, inshore SST was slightly warmer compared with offshore in the northern portion of the grid. In

contrast, coastal waters were slightly cooler in 2012 compared with the rest of the shelf. Water was warmest along the 200-line in 2011, leading to 2011 being the warmest year on average for our sampling sites (1.18 ± 0.70 ºC, versus 0.55 ± 0.49 and 0.047 ± 0.89 ºC for 2010 and 2012, respectively), corresponding to the year of earliest sea ice retreat. Minimum SST was measured along the 200-line in 2012, the same line where the survey's warmest water was observed the year before. Salinity followed a consistent trend of lower values inshore, partly reflecting the higher coastal contribution of sea ice melt in the years sampled (Fig. 3). However, salinity is also influenced by meteoric water (glacial melt and precipitation), which was also greatest nearshore. Oxygen isotope ratios in surface seawater show that meteoric water fraction in coastal waters (<50 km from the coast) was higher in 2011 than in 2012 (Fig. 3). In 2011, when coastal SST was warmer, the average meteoric water fraction was 1.20 %, compared with 0.77 % in 2012.

Sea ice seasons here are referred to by the LTER cruise that followed (i.e. 2010 ice year covers Feb 2009 – Feb 2010, the winter preceding the January 2010 sampling campaign). All three years showed shorter duration of sea ice cover relative to the 1978-2013 mean (Meredith et al., 2016), with 2011 having the shortest duration of cover (144 d), due primarily to the earlier ice retreat (~40 days earlier than 2010 or 2012). Sea ice cover reached an average maximum spatial extent in the first two years of the study, and greater extent in 2012 (Meredith et al., 2016). Oxygen isotope data (Meredith et al., 2013, 2016) indicate a southward propagation of sea ice in both 2011 and 2012 (Fig. 3; no data available for 2010); more freezing occurred in the northern section of the grid and more melting in the southern region. The greatest seasonal SSS range was observed in 2011, when southward propagation was greatest. There was slightly reduced southward movement in 2012, but consistent with the greater maximum ice extent, the contribution of sea ice melt water to surface waters was greater in 2012 (0.67 ± 0.77 %) than in 2011 (0.27 ± 0.71 %).

3.2 Trace metal distributions: Iron

Overall, surface dissolved Fe (dFe) concentrations varied over a large range (0.02 – 7.82 nmol kg^{-1}; mean 0.37 ± 0.82 nmol kg^{-1}, median 0.15 nmol kg^{-1}, n=231). High concentrations were observed in coastal samples, with the strongest enrichment near the

southern edge of Marguerite Bay in 2011 where the maximum dFe of 7.82 nmol kg^{-1} was observed (Fig. 4; Supplementary Fig. S1). Higher dFe relative to other years was present throughout this line (+100), while dFe enrichment on other sampling lines was restricted to coastal stations. Most sampling lines showed coastal enrichment in all years, although this was most pronounced in 2011.

Beyond the shelf break, in contrast, dFe was very low (0.19 ± 0.27 nmol kg^{-1}, n=71, samples seaward of the 500 m isobath) in all three sampling years. In some years, low concentrations were present in surface waters over the shelf, as close as ~25 km from the coast (Fig. 4). Overall, dFe was <0.20 nmol kg^{-1} in 57% of stations sampled, and <0.10 nmol kg^{-1} in 35%.

Distributions of particulate Fe (pFe) also showed a very large range, from <0.20 nmol kg^{-1} to >40 nmol kg^{-1} (overall average 2.3 ± 4.5 nmol kg^{-1}, median 0.78 nmol kg^{-1}, n=177), with low values near and beyond the shelf break and the highest concentrations inshore (Fig. 4). These are the first Fe data for the central WAP shelf south of Adelaide Island (67.34ºS), and they show that the WAP shelf is characterized by large regions with very low surface dFe and pFe concentrations. As an example, pFe averaged 0.68 ± 0.93 nmol kg^{-1} (n = 113) in samples collected near the shelf break (within 75 km of the 500m isobath). However, this value excludes additional samples where very low pFe led to sample signals being comparable to filter blanks (see Methods), thus the true average is even lower.

The trend of coastal dFe enrichment was also seen in pFe, with a maximum observed in 2011, although for pFe the highest concentration was located in northern (200 line), not southern (+100 line) Marguerite Bay, and was thus displaced from the dFe maximum (Fig. 4). Particulate Fe was also high in this location in 2012, as well as inshore on the adjacent 300 sampling line. Additionally, in all years, moderate pFe enrichments were observed in surface waters of Palmer Deep (coastal 600 line) and in coastal stations of the southernmost sampling lines (000 and -100 lines).

3.3 Trace metal distributions: Manganese

Although Mn and Fe have several common sources and sinks, the dMn distribution in WAP surface waters (Fig. 5) was different from that of dFe in several

respects. While both elements decreased in concentration with distance from the coastline this decline was more gradual for dMn than for dFe. The very high dFe values in southern Marguerite Bay 2011 are not reflected in dMn concentrations, though dMn enrichments above Palmer Deep persisted analogously to dFe in all three years (Fig. 5). In addition, 2012 data showed average dMn (1.22 ± 0.70 nmol kg^{-1}) ~2-fold higher than in other years (0.69 ± 0.43 and 0.67 ± 0.48 nmol kg^{-1}, 2010 and 2011, respectively; Fig. 5), whereas the average dFe in 2012 (0.15 ± 0.14 nmol kg^{-1}) was approximately half that of the earlier seasons (0.26 ± 0.19 and 0.31 ± 0.33 nmol kg^{-1} in 2010 and 2011, excluding very high values > 2 nmol kg^{-1}; Fig. 4). In contrast, pMn distributions were very similar to those of pFe with strong enrichment in northern Marguerite Bay in 2011 and Adelaide Island in 2012, relatively high values near Palmer Deep and central Marguerite Bay, and low values throughout most of the region in 2012.

3.4 Trace metal distributions: Particulate Al and Ti

The lithogenically-sourced metals Al and Ti were also measured in suspended particles. Particulate Al ranged from 0.07 - 135 nmol kg^{-1}, with consistently low values measured in samples near and beyond the shelf break (Fig. 6). The range of pTi was 0.02 – 4.16 nmol kg^{-1} (not shown). For both, concentrations were highest in the same years and locations as for pFe: Marguerite Bay in 2011, Adelaide Island in 2012, and to a lesser extent Palmer Deep and inshore on the southern sampling lines in all years. As for pFe, low concentrations were most widespread over the shelf in 2012 relative to the other sampling years.

Ratios of Fe:Al and Fe:Ti displayed across-shelf gradients but distinct spatial distributions with variable and often non-monotonic trends with distance from shore, with Fe:Al being more variable. Comparing inter-annual means, Fe:Al was lower on average in 2010 with the highest ratios measured in 2012. The cross-shelf gradients in Fe:Al were not spatially consistent, with both minima and maxima observed in mid-shelf surface waters (Fig. 6). In contrast, Fe:Ti ratios showed a more consistent trend from higher inshore values to lower off-shelf values, with most samples having a ratio <10 mol:mol. Ratios >10 mol:mol were found only on the inshore portion of the 200-line in 2012 (Fig. 6). Overall Al:Ti ratios were below average upper crustal values (34.8 mol:mol,

McLennan, 2001), and distributions of Al:Ti were similar to the trends in Fe:Ti, with increasing values found inshore and higher values near Marguerite Bay in 2011 and 2012 (Fig. 6). In some instances the distributions of Al:Ti and Fe:Ti differed markedly. For example, on the 500 sampling line in 2012, Al:Ti ratios were low relative to surrounding samples, whereas Fe:Ti ratios were high.

3.5 Trace metals in meteoric melt water

Concentrations of dissolved Fe and Mn determined from a meltwater stream are presented in Table 2, giving an indication of endmember concentrations of these metals from meteoric sources, which were much higher than the concentrations found in seawater.

4. Discussion

Despite the hypothesized role of the WAP shelf as a source region of Fe to the greater Southern Ocean (De Jong et al., 2012), no previous studies have investigated Fe concentrations throughout the WAP shelf; the majority of measurements are from the northern tip of the peninsula and the arc of subantarctic islands from the South Shetland Islands to South Georgia. Here we present the first investigation of the large-scale horizontal and temporal distribution of trace metals in WAP shelf surface waters, and consider spatial trends and interannual variability to investigate the main sources and sinks controlling surface metal distributions throughout the Pal-LTER grid.

4.1 Potential Fe sources to the WAP shelf

While atmospheric dust is commonly considered the dominant Fe source to the global ocean (Jickells, 2005), the iron flux from atmospheric dust is very low over the Southern Ocean as a whole (Gao et al., 2001; Tagliabue et al., 2009; Wagener et al., 2008), although in the WAP region there is potential for some local inputs adjacent to areas of exposed rock and glacial flour. In the absence of measured dust fluxes, daily dust deposition was estimated at 0.005 – 0.01 mg m^{-2} for our sampling grid (Wagener et al., 2008). To obtain a maximum possible dust Fe contribution we used average crustal Fe content and a high Fe solubility estimate of 10% (following De Jong et al., 2015), which equates to annual dFe accumulations of 5 - 10 pmol kg^{-1} dFe, and 44 – 87 pmol kg^{-1} pFe if fully retained in the summer mixed layer (average mixed layer depth 24 m in 2012, Eveleth et al., 2016). Even following the extreme assumption of zero uptake or scavenging loss of dust-derived dFe, dust deposition of this magnitude could only account for at most half of the observed pFe in offshore samples with very low pFe of ~200 pmol kg^{-1}. Thus, atmospheric input is unlikely to contribute significantly to trace metal supply to the WAP, consistent with other studies from the wider WAP, Southern Ocean, and high latitudes in general (De Jong et al., 2015; Duce et al., 1991; Gao et al., 2001; Tagliabue et al., 2017).

Thus, additional Fe must be supplied to the WAP shelf from terrestrial and marine sources. For the purposes of this discussion, we will differentiate terrestrial from marine sources of Fe. Terrestrial sources include subglacial meltwater, glacial melt delivered

directly to the ocean or via meltwater streams over exposed rock, and terrestrial precipitation, which may acquire additional Fe as it flows to the coast. Marine Fe sources include sea ice, resuspension of shelf sediment, and diffusive fluxes from reductive or non-reductive sedimentary Fe dissolution. Inputs from resuspension processes within cavities beneath ice shelves are considered terrestrial here, as the lithogenic material present is derived from land, and sedimentary redox processes fueled by organic matter fluxes beneath these ice shelves are expected to be much less active than in fully marine sediments underlying more productive, open waters.

To investigate the relative significance of terrestrial vs. marine Fe sources, we investigated patterns of interannual Fe variation and instances of pronounced Fe enrichment, since instances of low Fe concentration could indicate either comparatively low Fe input or biological uptake and vertical export. We focus the analysis on 2011, which displayed the greatest spatial variability in both dFe and pFe, and on 2012 which had similar spatial coverage. We consider primarily the southernmost sampling line near Charcot Island (-100 line), the southern Marguerite Bay line (+100 line) where the highest dFe was observed (7.8 nmol kg^{-1}; +100 line; Fig. 4), Northern Marguerite Bay (200 line) with the highest pFe values (42 nmol kg^{-1}), and Palmer Deep (inshore 600 line) where moderate dFe enrichment was present in all sampling seasons.

4.1.1: Sea ice

Iron concentrations, both dissolved and particulate, showed little correlation with contributions of sea ice melt water to surface waters (Fig. 7d, g, j). On an annual and regional level, sea ice extent and sea ice melt fraction in the Pal-LTER grid was greater in 2012 than in 2011 (Meredith et al., 2016; Fig. 3), whereas average dFe was lowest in 2012 (Fig. 4). In 2012, low dFe implies low Fe supply (or alternatively, high biological uptake, which is not supported by the biological data - *see Section 4.3.4*), which argues against a significant sea ice Fe source.

The nearshore Fe enrichment on the -100 sampling line in 2011 can be distinguished from inputs at more northern samples by the minimum in salinity (Fig. 7a, b). While this southern sampling line was likely to be most strongly influenced by sea ice in 2011 given its southward propagation in this year (Meredith et al. 2016), the

correlation between Fe (both dissolved and particulate) and sea ice contributions was weaker than for meteoric inputs (Fig. 7c, d). Along the +100 sampling line dFe and pFe showed strong correlations with the water column/mixed layer proportions of both sea ice and meteoric water (Fig. 7g, h), but here too the relationship was statistically stronger with meteoric inputs than with sea ice inputs. To produce the observed distributions of surface seawater dFe, pure sea ice melt would have to contain ~400 nmol kg^{-1} dFe. Although sea ice is enriched in dFe relative to sea water (as well as total dissolvable Fe and pFe), measured dFe concentrations in sea ice cores are much lower (0.2 – 109 nM; e.g.: Lannuzel et al., 2014, 2007; Schallenberg and Lannuzel, 2016; Van Der Merwe et al., 2011). As such, sea ice is unlikely to be the dominant driver of the high dFe concentrations.

The Palmer Deep area (inshore 600-line) was also a location of elevated dFe and pFe in all years (Fig. 4), with the greatest enrichment seen in 2011. In this region, Fe concentrations and meteoric fractions were concurrently greatest in 2011, whereas sea ice melt was higher in 2012 (Fig. 3). This suggests that meteoric/glacial processes were also more important than sea ice melt for supplying Fe in this northern region, further indicating that sea ice was not a primary driver of Fe distributions.

Typical dFe enrichment in sea ice relative to underlying water (~10-fold; Lannuzel et al., 2014a, 2014b, 2007; Schallenberg and Lannuzel, 2016) and the sea ice melt fraction in surface waters (0.46 ± 0.77%, max = 2.8 %) suggest that average sea ice dFe contributed only ~5 % of measured seawater dFe in WAP surface waters. In the offshore portion of the Pal-LTER grid, in contrast, sea ice has the potential to be a significant Fe input, as the ambient concentrations were much lower (~70 pmol kg^{-1}). For example, at the offshore end of the -100 line, an increase in sea ice melt fraction from 0 % to 2 % with negligible change in meteoric content was accompanied by a 60 pmol kg^{-1} increase in dFe (2011). This equates to ~3 nmol kg^{-1} dFe for pure sea ice melt (and 7.5 nmol kg^{-1} pFe), consistent with published values of sea ice Fe concentrations (Lannuzel et al., 2011, 2010, 2007; van der Merwe et al., 2011), accounting for almost 50% of seawater dFe at this location. In addition, movement of Fe-rich fast ice from inshore regions to open ocean waters (Lannuzel et al., 2014; Van Der Merwe et al., 2011)

may serve as a significant Fe source to potentially Fe-limited surface waters of the adjacent ACC.

Our analysis points to an overall minor role for sea ice Fe inputs along the WAP shelf. However, we used a combination of $\delta^{18}O$ and salinity to trace sea ice meltwater, which produces a distribution for sea ice melt that may differ from the distribution of a brine-mediated Fe source, since dFe released with sea ice brine drainage may enter the water column prior to and in a different location than pFe associated with the main pulse of low-salinity melt water (Lannuzel et al., 2013; van der Merwe et al., 2011). Variable exchange of seawater with high-salinity brine, and/or increased porosity prior to complete ice melt could further decouple the inputs of brine (and dissolved metals) from bulk meltwater, temporally, spatially, or both. More measurements of Fe in sea ice, brine, and underlying waters prior to and during melting are needed to better assess the magnitude and distribution of sea ice Fe sources to surface waters.

4.1.2 Glacial processes and precipitation

Throughout the study area, Fe concentrations were strongly correlated with meteoric water inputs (Fig. 7e, h, k), suggesting that lithogenic particulate and dissolved Fe originate from glacial melt and/or precipitation. In 2011, the +100 sampling line in southern Marguerite Bay had the highest measured dFe concentrations of this study (8.2 nmol kg^{-1}). While sea ice would have to contain unreasonably high Fe concentrations to explain this enrichment, a meteoric meltwater endmember of ~300 nmol kg^{-1} would account for the observations, which is in very much in line with glacial meltwater Fe concentrations sampled near Palmer Station (Table 2).

To investigate spatial variability in glacial contributions of Fe to WAP surface waters, we compared the relationship between dFe, pFe, and meteoric water for several sampling lines in 2011 (Table 3). Concentrations of both dFe and pFe estimated for a pure meteoric meltwater endmember varied by a factor of ~30 across the LTER sampling grid. Along the +100 line the correlation with meteoric water was very strong, and showed greater dFe additions per unit melt than in any other samples (3.02 nmol kg^{-1} per % meteoric water for this transect, compared to 0.26 nmol kg^{-1} for the -100 line, Table 3 and Supplementary Information). In contrast to all other sampling lines, dFe on

the +100-line was enriched to higher absolute concentrations than pFe, implying higher dFe than pFe in the local meteoric endmember (Table 3). This may be attributable to small but variable proportions of Fe-rich subglacial water (Death et al., 2014), ice-shelf cavity processes, and/or meltwater and precipitation acquiring Fe as they flow over exposed areas of rock or sediment, all of which can be expected to vary spatially and temporally. Although these Fe-rich endmembers likely exemplify a small component of total meteoric water (McGillicuddy et al., 2015), small changes in such high-Fe waters can significantly affect metal delivery from glacial processes.

Outflow from the George VI ice shelf at the southern end of Marguerite Bay veers westward (Jenkins and Jacobs, 2008; Potter et al., 1988) towards the inshore end of our +100 sampling line. Therefore, an ice-shelf derived signal on the +100 line is consistent with local circulation patterns. Few measurements of glacial dFe and pFe concentrations have been made in the WAP region, but a range of 24-157 nmol kg^{-1} total Fe from Talos Dome ice cores (East Antarctica, Spolaor et al., 2013) and 32 % solubility of pFe (Edwards et al., 2001) equates to dFe and pFe contributions of 0.18 – 1.2 and 0.39 – 2.6 nmol kg^{-1}, respectively, based on a 2.4 % meteoric water component (at the inshore end of the +100 line, Fig. 7i). These estimates are insufficient to explain the high dFe or pFe seen in the +100-line samples. However, meteoric water may also include subglacial water that has interacted with the bedrock and sediments beneath the glacier. Although poorly constrained, data suggest that subglacial dFe can be 2-3 orders of magnitude higher than in glacial meltwater (see reviews in Death et al., 2014; Wadham et al., 2013). If we assume that particulate Fe is enriched to a lesser extent (only 1 order of magnitude, to account for sinking) in subglacial water relative to glacial meltwater, and that 5 % of meteoric water is subglacial (following McGillicuddy et al., 2015), 2.4 % meteoric water in seawater could provide 5.2 – 340 nmol kg^{-1} dFe and 11.3 – 74 nmol kg^{-1} pFe, enough to supply the measured Fe in our +100 line samples (even at lower subglacial contributions), as well as explain the greater enrichment in dFe relative to pFe in this region.

Alternatively, upwelling of CDW beneath George VI Ice Shelf, with additions of glacial meltwater, inputs of subglacial water, and possible sedimentary sources driven by dynamic processes near the grounding line may also explain the high dFe seen here. Such

a mechanism has been inferred for the Dotson Ice Shelf in the Amundsen Sea (Sherrell et al., 2015) and could entrain particulate and dissolved metals without necessarily requiring redox-mediated source processes. Meltwater fluxes are discharged from George VI Ice Shelf primarily into George VI Sound, which then mixes with southern Marguerite Bay waters (Jenkins and Jacobs, 2008). Marguerite Bay surface waters intrude into northern George VI Sound in the east, exiting to the west, with strong vertical mixing (upwelling and downwelling) in this region (Dorland and Zhou, 2008). Thus, subglacial water and processes occurring within the cavity may all contribute to the Fe enrichment on the +100 line, analogously to processes likely occurring near Pine Island Glacier and the Dotson ice shelves in the Amundsen Sea (Gerringa et al., 2012; Sherrell et al., 2015).

The low concentrations of dMn in 2011 in coastal samples on the -100 line (0.44 ± 0.12, n = 8; <100 km from the coast) and the entire +100 sampling line (0.67 ± 0.18 nmol kg^{-1}, n = 15; Fig. 5) further support minimal input from sediments along these sampling lines. Dissolved Mn:Fe was low in coastal (<100 km from shore) samples along the +100 line (0.41 ± 0.38 mol:mol) and the -100 line (1.0 ± 0.33 mol:mol; Fig. 8). Reductive processes in marine sediments favor the dissolution and release of Mn before Fe (Froelich et al., 1979). Combined with the longer residence time of dMn than dFe, the low dMn:dFe observed here indicates a non-reductive source from crustal material, which has a very low mean Mn:Fe content (0.017 mol:mol; Taylor and McLennan, 1995). The coincident low salinity supports significant meltwater (sea ice or glacial; Figs. 3, 7) influence at the surface, suggesting delivery of crustal material via meltwater processes.

Overall, meteoric water was 40% lower on average in 2012 compared to 2011 throughout the grid (Section 3.1). The outer portion of the shelf was low in dFe and meteoric water in both years. The most striking interannual difference, however, occurred in mid- and inner-shelf waters. Near the coastline (<30 km), meteoric contributions were 1.37 ± 0.59 % in 2011 and 0.83 ± 0.51 % in 2012. The relatively small difference in meteoric input of 0.54 % and a difference in dFe of 0.55 nmol kg^{-1} (0.86 ± 1.0 nmol kg^{-1} in 2011, excluding the 2 samples >4 nmol kg^{-1}, versus 0.31 ± 0.21 nmol kg^{-1} in 2012) implies a meteoric dFe concentration of 102 nmol kg^{-1} (assuming no dFe loss to nearshore waters proximal to the source), which is in keeping with a source mechanism

involving dFe-enriching subglacial processes (Death et al., 2014; Wadham et al., 2013) as well as glacial meltwater streams (Table 2).

However, we must also explore the possibility that a greater contribution of sedimentary Fe from upwelling or mixing in shallow waters produces the observed trends, independent of meteoric processes. As meteoric input and proximity to upwelled or resuspended sediment both tend to be greatest at the coast, the spatial patterns of Fe and Al do not allow differentiation between terrestrial and marine sediment sources of particulates. Thus, we next consider trends in Mn as a proxy for marine sedimentary processes.

4.1.3 Marine sedimentary input

Low oxygen conditions in upper sediments underlying productive surface waters may drive the release of sedimentary Mn(II) along with Fe(II), as seen near the South Shetland Islands (Hatta et al., 2013). Because Fe (II) is subject to faster oxidation (Millero et al., 1987) and greater scavenging in the upper sediment column and overlying waters (Measures et al. 2013), dMn should be a good qualitative tracer for the presence of reductive dFe release. Hatta et al. (2013) found greater Mn:Fe release during summer conditions than for stronger winter current flow. Gradients in dMn across the WAP shelf were consistent with sedimentary fluxes being strongest at the coast, more intense in the northern portion of the grid in 2011, and highly variable between years.

Although the dMn signal may also be supplied by meteoric water, this would require 105 nmol kg^{-1} (northern lines, 2012) to 124 nmol kg^{-1} (600-line, 2011) in endmember meteoric water to account for the observed dMn distribution. This is 3-4 times higher than dMn measured in glacial melt streams at Palmer Station (Table 2), suggesting that most dMn must come from another source. However, the two meltwater samples reported here are most likely a mix of snow and glacial ice melt, and they were sampled near the snowline in a stream that flowed over exposed rock and sediment before reaching the coast. Therefore, these concentrations may not be representative of average meltwater metal content, since precipitation may alter metal concentrations relative to pure glacial melt additional metals may be acquired along the flow path, and high sediment load in meltwater may scavenge metals, altering concentrations before

meltwaters enter the sea. Recent data from King George Island give a wide range of dMn:dFe in iceberg melt (0.01-16 mol:mol; Kim et al., 2015). This range highlights the need for additional measurements to better constrain trace metal concentrations in Antarctic meltwaters. Marine sediments are a more likely source of Mn to coastal waters in this productive region, consistent with northern WAP studies (Hatta et al. 2013, Measures et al. 2013).

In agreement with the inference of enhanced marine sediment influence on the Marguerite Bay/Adelaide Island samples, particulate Fe:Ti ratios were higher in 2011 along the 200 line (and the 300 line, 8.7 to > 10 mol:mol) compared to the -100 line (7.1 ± 1.0 mol:mol; Fig. 6). The Fe:Al ratios were also slightly higher in the 200-300 line particulate samples (~0.3-0.35 mol:mol, versus 0.24 for the +/-100 lines), suggesting a source enriched in Fe relative to both crustal Al and Ti in the Marguerite Bay/Adelaide Island samples, consistent with increased influence of sediments in this region. An Fe source from an authigenic oxide-rich shelf sediment to deep waters could increase both Fe:Ti and Fe:Al ratios, and sediment work in Palmer Deep has measured residual (refractory) Fe:Ti of 6.4 mol:mol, versus Fe:Ti of 267-422 mol:mol in the oxide fraction (Kryc et al., 2003). Palmer Deep sediments also displayed high Fe:Al relative to crustal ratios, in both the exchangeable (0.54 – 1.6 mol:mol) and oxide (0.56 – 1.1 mol:mol) fractions (Kryc et al. 2003). The trend to higher inshore Al:Ti along the 200 line further suggests greater oxide proportions in particulate matter, with this fraction being enriched in Al relative to Ti (400 - 475 mol:mol) relative to residual and organic particulates (23 - 29 mol:mol; Kryc et al. 2003). The eastern end of the 200 line surface transect lies above the northern edge of Marguerite Trough and ~20 km from a small island; the complex bathymetry and circulation may result in vertical mixing of resuspended sediment and pore water from shallow depths. A small proportion of this marine sediment-derived signal mixing to the surface would thus explain the modest differences in dMn, dMn:dFe, pFe:pAl and pFe:pTi between the 200 and more southerly sampling lines.

In 2011, dissolved Mn was highest along northern sampling lines, suggesting that sediment processes contributed to metal availability to a greater extent in the northern portion of the grid that year. Inshore (<100 km from the coast) dMn averaged 1.10 ± 0.52 nmol kg^{-1} across the northern (300-600) lines, compared to 0.63 ± 0.37 nmol kg^{-1} for

lines -100 to 200. These averages consider only inshore samples where meteoric and shallow sediment fluxes were greatest, but the pattern is consistent even when all stations are included (Fig. 9a). The higher average inshore dMn:dFe for northern lines (5.9 ± 3.6 mol:mol, versus 1.2 ± 1.2 mol:mol for southern lines; Fig. 9b) is also consistent with greater metal fluxes driven by sediment redox processes in the north. Given the greater number of ice-free days in the northern portion of the grid, allowing for higher seasonal primary productivity and export, we suggest that the pattern of higher dMn along the northern lines reflects the spatial delivery of organic matter to the sediments (greater in the north), driving greater oxygen consumption, shallower oxygen penetration, and greater efflux of reduced Mn during early diagenesis (Hatta et al. 2013). This process would also drive reductive dissolution of Fe, but the oxic water column might limit efflux of dFe through rapid reoxidation of Fe(II) and subsequent scavenging and precipitation near the sediment-water interface.

These data further imply a much greater sedimentary input in 2012, when dMn was highest (Fig. 9d), and dMn:dFe was almost 3 times the 2011 value: 14.6 ± 10.5 (n=35) versus 5.3 ± 3.7 (n=29). However, the high Mn in 2012 was not reflected in surface Fe concentrations, as low dFe conditions were widespread in this sampling year. We thus infer that different relative contributions of glacial (high-Fe) and sedimentary (high-Mn) fluxes were the likely drivers of the variable Mn:Fe ratios observed in 2011 and 2012. Overall, inshore dFe and pFe were greatest in 2011, coinciding with the greatest meteoric water contributions to surface waters, but lower sea ice melt and dMn. The inverse was true for 2012: higher sea ice melt and dMn, lower meteoric component and low Fe (Fig. 3-5). Therefore, glacial processes appear to exert the greatest control on surface Fe concentrations throughout this region of the WAP.

4.2 Shelf break signal

We also identify an intriguing signature above the shelf break along the -100 sampling line in 2011, based on surface dMn concentrations at ~100-150 km from shore (Fig. 11). Off-shelf samples were very low in dMn (mean = 54 ± 44 pmol kg^{-1}, n=6), while those near shore (<100 km from the coast) averaged 440 ± 120 pmol kg^{-1} (see Fig. 11). In samples above the shelf break (100-150 km from shore, 500 m isobath is at ~125

km), dMn was markedly higher than in offshore or coastal samples, at 680 ± 360 pmol kg^{-1}.

Higher dMn has also been observed at the southern boundary of the ACC in the Weddell Sea (Middag et al., 2011), attributed to hydrothermal sources. However, hydrothermal or other sources of dMn (photoreduction, atmospheric deposition, or meltwater) are unlikely to vary sufficiently over the scale of our transect and thus are insufficient to explain the shelf break enrichment in dMn. As a result, high dMn is best explained by vertical mixing of a sedimentary input. We note that this signal may be subject to significant lateral transport before being brought to the surface, so the sedimentary source need not be in the shelf break vicinity. Supporting this mechanism, the available CTD profiles show reduced vertical density gradients offshore, presenting a weaker barrier to vertical mixing than in mid-shelf or inner-shelf regions (not shown). The high Mn:Fe ratios observed above the shelf break also indicate a marine sediment source (Fig. 11c), in contrast to the lower Mn:Fe ratios nearer land indicative of meteoric inputs. Similar to the inshore sampling locations where high dMn concentrations suggested a marine sediment influence, dFe enrichment was also absent from the shelf-break locations.

Over the full sampling region, maximal Mn:Fe ratios correspond to the shelf break or canyon features (shown by the 500 m isobath) on most sampling lines (Fig. 8). At this distance from the coast and in areas of low or inconsistent sea ice contributions, these ratios may reflect turbulent vertical mixing associated with the shelf break, bringing dissolved and particulate matter from deeper waters to the surface. Given the depth of the shelf break (~500 m), this signal most likely reflects dissolved and particulate material from just below the mixed layer, rather than sediments from the underlying shelf break. Particulate matter may be concentrated by a strong pycnocline across the WAP shelf, allowing time for authigenic mineral formation, remineralisation into dissolved forms, and loss of the most dense particles, before it is advected into the frontal mixing zone and redistributed vertically. Such material would likely be present in subsurface layers throughout the region, and upon reduction in stratification induced by frontal mixing would be mixed to the surface at the shelf break. This interpretation can be tested in the

future by evaluating variations in particulate elemental ratios with depth near the shelf break compared to shelf regions where stratification is stronger.

4.3 Iron sinks

A key observation of this study is the low concentration of dFe and pFe throughout most of the grid in 2012, and in substantial portions of outer shelf waters in other years. Although low dFe is an established characteristic of surface waters in the open ACC, our results demonstrate that very low dFe extends far onto the shelf: dFe was <0.1 nmol kg^{-1} in 9 samples within 75 km of the coast. In these same samples, pFe was also low (0.76 ± 0.88 nmol kg^{-1}; n = 5). Overall, dFe concentrations in 2012 were only 25 % of those in 2011 (0.15 ± 0.14 nmol kg^{-1}, n = 101, 2012; versus 0.62 ± 1.20 nmol kg^{-1}, n = 100, 2011).

The most likely explanation for the low dFe in 2012 is lower glacial input in this year, as outlined above. However, consideration of Fe distributions with respect to sources must be balanced by assessment of removal processes. In addition to rapid scavenging of sedimentary Fe, biological drawdown is also a significant control on dFe in WAP surface waters (Bown et al., 2016). For example, high biological activity coincides with the significant dFe enrichment observed inshore on the +100 line in 2011 (Fig. 4, supplementary material Fig. S2), and would likely have depleted dFe in this location given continued productivity following sampling. However, although chlorophyll concentrations were elevated inshore on the northern gridlines in 2012, biological uptake is unlikely to be the dominant driver of low dFe in 2012, as primary production and N drawdown (nitrate plus nitrite) in this region were similar in 2012 and 2011 (supplementary material Fig. S2). Along the southern gridlines (200-line and southwards), chlorophyll, primary production, and N drawdown were all much lower in 2012 than in 2011, consistent with later ice retreat in 2012. Overall, while biological drawdown will certainly affect surface distributions of dFe, the widespread low-dFe conditions in 2012 are likely to predominantly reflect lower input from meteoric sources dominated by glacial processes.

Our observations raise the possibility that the low dFe concentrations typically associated with offshore ACC waters can also limit phytoplankton productivity on the

WAP shelf in January. Although coastal processes can deliver substantial Fe, as seen here (and in Annett et al., 2015; Bown et al., 2016), this signal is attenuated quickly with distance offshore. It is apparent from Fig. 10 that dFe behaves differently from dMn with distance from the coast. Dissolved Mn follows a linear trend with distance, and suggests quasi-conservative mixing with low-Mn ACC water. In contrast, dFe is lost rapidly due to physical processes (and potentially biological uptake), but is stable at 110 ± 70 pmol kg^{-1} at distances greater than 30 km from shore (from Fig.10b; the average is similar for the full dataset, excluding the extremely high dFe on the 200-line in 2011: 170 ± 140 pmol kg^{-1}, n=183). This suggests that at low concentrations, dFe may be controlled primarily by biological processes including cellular uptake, remineralization, or stabilization by complexation with organic ligands. Little is known about ligand distribution or cycling on the WAP shelf though some data are available for the South Shetland Islands (Buck et al., 2010; Jiang et al., 2013a) and Amundsen Sea (Thuróczy et al., 2012). A full treatment of biological metal uptake on the WAP will be considered in a separate publication.

Throughout the Pal-LTER grid sampled here, pFe is greater than dFe in nearly all samples (Fig. 4). In areas of low and potentially limiting dFe concentrations, Fe from the particulate phase may provide an additional Fe source to phytoplankton communities, and recent evidence suggests glacial pFe may be a significant component of bioavailable Fe to the Southern Ocean (Raiswell et al., 2016). However, potential Fe limitation is further complicated by bioavailability; some fraction of particulate and colloidal Fe may be available to phytoplankton (Chen and Wang, 2001; Raiswell et al., 2016), and biological processes involving bacteria or grazers can modulate bioavailability (Shaked and Lis, 2012), which differs even between dissolved species of Fe (Lis et al., 2014).

Spatially heterogeneous Fe inputs as documented here, coupled with strong biological control where dFe is low would support the hypothesis of patchy Fe limitation in WAP shelf waters (Garibotti et al., 2003; Prézelin et al., 2004; Smith et al., 2008). However, throughout the WAP, phytoplankton distributions are also strongly influenced by variables such as mixed layer depth, light, stratification and bathymetry (Carvalho et al., 2016; Ducklow et al., 2013; Kavanaugh et al., 2015; Vernet et al., 2008). Consequently, we highlight the need for incubation experiments or tracer studies of Fe

stress to fully assess the degree and spatial pattern of phytoplankton Fe stress or limitation across the WAP shelf euphotic zone.

4.4 Future changes in Fe supply

Along the WAP, >80 % of glaciers have retreated since 1950 and rates of retreat are accelerating (Cook et al., 2016; Davies et al., 2014; Pritchard and Vaughan, 2007). The duration of winter sea ice cover has also decreased drastically (by 3.3 months between 1979 and 2011; Stammerjohn et al., 2012). Such processes are likely to have an impact on Fe dynamics on the central WAP shelf. Our results show a small role for sea ice Fe input, spatially and temporally variable sedimentary signals that are associated with minor or local Fe supplies, and a dominant Fe input from meteoric sources.

Only a fraction of sedimentary Fe is likely to be mixed upwards to the surface where our samples were collected. In contrast, meteoric meltwater is delivered higher in the water column, and surface runoff is supplied directly to the surface waters. Full water-column sampling may reveal a greater role for sedimentary Fe fluxes at depth, but the surface samples presented here imply relatively minor and spatially heterogeneous net dissolved Fe fluxes from reducing marine sediments. Additionally, sedimentary trace metal fluxes from non-reductive processes may not be reflected in dMn distributions. As such, the contribution of non-reductive processes to the total sedimentary Fe fluxes to surface waters remains uncertain, but future studies of full water-column trace metal distributions may help to quantify the importance of reductive and non-reductive sedimentary sources relative to the key meteoric Fe sources identified here.

Unlike the other Fe supply mechanisms investigated here, melting sea ice can deliver Fe directly to offshore areas. Further, phytoplankton blooms often coincide with the retreating ice edge (Ducklow et al., 2013; Garibotti et al., 2005; Smith and Nelson, 1985) supplying Fe when it is most likely to be required by phytoplankton. In contrast to other regions of the Antarctic, sea ice along the rapidly-warming WAP has been declining in recent decades, with earlier retreat and markedly later advance (Parkinson and Cavalieri, 2012; Stammerjohn et al., 2008). Although sea ice derived Fe plays a minor role in inshore waters in summer, any future reduction in sea ice cover could strongly impact Fe supply to Fe-poor, offshore waters where the relative contribution of

sea ice Fe to the total surface Fe inventory is much greater, especially earlier in the season.

In addition to increased glacial meltwater and precipitation fluxes, changing glacial cover can affect the proportion of subglacial meltwater, as well as the extent of interaction of subglacial water or precipitation with underlying rock and sediment, allowing changing sediment load and mineral dissolution to affect dFe and pFe concentrations in meteoric waters. Increasing CDW incursions and on-shelf heat flux is increasing melt rates of ice shelves and marine-terminating glaciers and may increase Fe fluxes from subglacial cavities. On balance, it is reasonable to expect increasing meteoric and subglacial Fe supply with continued warming. However, we note that decreasing winter sea ice cover can result in deeper winter mixed layers that persist into summer (Venables et al., 2013), distributing meteoric-sourced Fe over a larger depth range. Thus, the net change in available Fe in the euphotic zone will depend on a combination of meteoric Fe concentrations, the balance of inputs from meteoric processes and marine sediment supply from below, any change in removal by scavenging in response to changes in particle load, the depth of winter mixing, and extent of summer stratification. The impact of any change in Fe supply will further depend on trends in the biological demand, the magnitude and even direction of which is uncertain (*e.g.* latitudinal variability with overall decline, Montes-Hugo et al., 2009; increasing, Moreau et al., 2015), as well as the degree of Fe limitation throughout the shelf euphotic zone. All of these factors need to be considered in predictions of future ecological changes and in the design of future observational programs.

5. Data

Trace metal data presented here will be made publicly available through the Biological and Chemical Oceanography Data Management Office (www.bco-dmo.org), and in the interim is available by request from the authors.

6. Acknowledgements

We are grateful to the captain and crew of ARSV *Laurence M. Gould*, as well as the USAP technicians, and all the scientific personnel who contributed to sample collection and help during at-sea repairs. The support of Palmer LTER lead scientist Hugh Ducklow is greatly appreciated. We would also like to thank members of the Sherrell and Schofield labs who helped with cruise preparation, and Paul Field for his help with mass spectrometry during the sample analyses. We are also grateful to the journal editors and two anonymous reviewers whose careful comments improved the manuscript. This work was funded by the US National Science Foundation (ANT-0838995 to R.M.S. and ANT-0823101 to O.S.). Field cruise support, hydrographic data and $H_2{}^{18}O$ sampling were supported by NSF ANT-0823101 and the Palmer LTER program.

6. References

Annett, A.L., Skiba, M., Henley, S.F., Venables, H.J., Meredith, M.P., Statham, P.J., Ganeshram, R.S., 2015. Comparative roles of upwelling and glacial iron sources in Ryder Bay, coastal western Antarctic Peninsula. Mar. Chem. 176, 21–33. doi:10.1016/j.marchem.2015.06.017

Ardelan, M. V., Holm-Hansen, O., Hewes, C.D., Reiss, C.S., Silva, N.S., Dulaiova, H., Steinnes, E., Sakshaug, E., 2010. Natural iron enrichment around the Antarctic Peninsula in the Southern Ocean. Biogeosciences 7, 11–25. doi:10.5194/bgd-6-7481-2009

Atkinson, A., Siegel, V., Pakhomov, E.A., Rothery, P., 2004. Long-term decline in krill stock and increase in salps within the Southern Ocean. Nature 432, 100–103. doi:10.1038/nature02950.1.

Bolmer, S., Beardsley, R.C., Pudsey, C.J., Morris, P., Weibe, P., Hofmann, E., Anderson, J., Maldonado, A., 2004. A high-resolution bathymetry map for the Marguerite Bay and adjacent West Antarctic Peninsula shelf for the Southern ocean GLOBEC program. Woods Hole Oceanogr. Inst. Tech. Rep. WHOI-2004-, 78pp. doi:10.1017/CBO9781107415324.004

Bown, J., Laan, P., Ossebaar, S., Bakker, K., Rozema, P., Baar, H.J.W. De, 2016. Bioactive trace metal time series during Austral summer in Ryder Bay , Western Antarctic Peninsula. Deep. Res. Part II. doi:10.1016/j.dsr2.2016.07.004

Boyd, P.W., Jickells, T., Law, C.S., Blain, S., Boyle, E.A., Buesseler, K.O., Coale, K.H., Cullen, J.J., Baar, H.J.W. De, Follows, M., Harvey, M., Lancelot, C., Levasseur, M., 2007. Mesoscale Iron Enrichment Experiments 1993 – 2005: Synthesis and Future Directions. Science (80-.). 315, 612–618.

Bromwich, D.H., Nicolas, J.P., Monaghan, A.J., Lazzara, M.A., Keller, L.M., Weidner, G.A., Wilson, A.B., 2012. Central West Antarctica among the most rapidly warming regions on Earth. Nat. Geosci. 6, 139–145. doi:10.1038/ngeo1671

Buck, K.N., Selph, K.E., Barbeau, K.A., 2010. Iron-binding ligand production and copper speciation in an incubation experiment of Antarctic Peninsula shelf waters from the Bransfield Strait, Southern Ocean. Mar. Chem. 122, 148–159. doi:10.1016/j.marchem.2010.06.002

Carvalho, F., Kohut, J., Oliver, M.J., Sherrell, R.M., Schofield, O., 2016. Mixing and phytoplankton dynamics in a submarine canyon in the West Antarctic Peninsula. J. Geophys. Res. Ocean. doi:10.1002/2016JC011650

Chen, M., Wang, W.-X., 2001. Bioavailability of natural colloid-bound iron to marine plankton: Influences of colloidal size and aging. Limnol. Oceanogr. 46, 1956–1967. doi:10.4319/lo.2001.46.8.1956

Cook, A.J., Holland, P.R., Meredith, M.P., Murray, T., Luckman, A., Vaughan, D.G., 2016. Ocean forcing of glacier retreat in the western Antarctic Peninsula. Science (80-.). 353, 283.

Davies, B.J., Golledge, N.R., Glasser, N.F., Carrivick, J.L., Ligtenberg, S.R.M., Barrand, N.E., van den Broeke, M.R., Hambrey, M.J., Smellie, J.L., 2014. Modelled glacier response to centennial temperature and precipitation trends on the Antarctic Peninsula. Nat. Clim. Chang. 4, 1–6. doi:10.1038/nclimate2369

De Jong, J., Schoemann, V., Lannuzel, D., Croot, P., De Baar, H., Tison, J.L., 2012. Natural iron fertilization of the Atlantic sector of the Southern Ocean by continental shelf sources of the Antarctic Peninsula. J. Geophys. Res. Biogeosciences 117. doi:10.1029/2011JG001679

De Jong, J.T.M., Stammerjohn, S.E., Ackley, S.F., Tison, J.L., Mattielli, N., Schoemann, V., 2015. Sources and fluxes of dissolved iron in the Bellingshausen Sea (West Antarctica): The importance of sea ice, icebergs and the continental margin. Mar. Chem. 177, 518–535. doi:10.1016/j.marchem.2015.08.004

Death, R., Wadham, J.L., Monteiro, F., Le Brocq, A.M., Tranter, M., Ridgwell, A., Dutkiewicz, S., Raiswell, R., 2014. Antarctic ice sheet fertilises the Southern Ocean. Biogeosciences 11, 2635–2643. doi:10.5194/bg-11-2635-2014

Dorland, R.D., Zhou, M., 2008. Circulation and heat fluxes during the austral fall in George VI Sound, Antarctic Peninsula. Deep. Res. Part II Top. Stud. Oceanogr. 55, 294–308. doi:10.1016/j.dsr2.2007.01.014

Duce, R.A., Liss, P.S., Merrill, J.T., Atlas, E.L., Buat-Menard, P., Hicks, B.B., Miller, J.M., Prospero, J.M., Arimoto, R., Church, T.M., Ellis, W., Galloway, J.N., Hansen, L., Jickells, T.D., Knap, A.H., Reinhardt, K.H., Schneider, B., Soudine, A., Tokos, J.J., Tsunogai, S., Wollast, R., Zhou, M., 1991. The atmospheric input of trace

species to the world ocean. Global Biogeochem. Cycles 5, 193–259. doi:10.1029/91gb01778

Ducklow, H., Fraser, W., Meredith, M., Stammerjohn, S., Doney, S., Martinson, D., Sailley, S., Schofield, O., Steinberg, D., Venables, H., Amsler, C., 2013. West Antarctic Peninsula: An Ice-Dependent Coastal Marine Ecosystem in Transition. Oceanography 26, 190–203. doi:10.5670/oceanog.2013.62

Dulaiova, H., Ardelan, M. V., Henderson, P.B., Charette, M.A., 2009. Shelf-derived iron inputs drive biological productivity in the southern Drake Passage. Global Biogeochem. Cycles 23, 1–14. doi:10.1029/2008GB003406

Duprat, L.P.A.M., Bigg, G.R., Wilton, D.J., 2016. Enhanced Southern Ocean marine productivity due to fertilization by giant icebergs. Nat. Geosci. 9, 219–221. doi:10.1038/ngeo2633

Edwards, R., Sedwick, P., Land, E., 2001. Iron in East Antarctic snow-Implications for atmospheric iron deposition and algal production in Antarctic waters. Geophys. Res. Lett. 28, 3907–3910.

Eveleth, R., Cassar, N., Sherrell, R.M., Ducklow, H., Meredith, M.P., Venables, H.J., Lin, Y., Li, Z., 2016. Ice melt influence on summertime net community production along the Western Antarctic Peninsula. Deep Sea Res. Part II Top. Stud. Oceanogr. doi:10.1016/j.dsr2.2016.07.016

Froelich, P., Klinkhammer, G.P., Bender, M.L., Luedtke, N., Heath, G.., Cullen, D., Dauphin, P., Hammond, D., Hartman, B., Maynard, V., 1979. Early oxidation of organic matters in pelagic sediments of the eastern equatorial Atlantic: suboxic diagenesis. Geochim. Cosmochim. Acta 43, 1075–1091.

Gao, Y., Kaufman, Y.J., Tanre, D., Kolber, D., Falkowski, P.G., 2001. Seasonal distribution of aeolian iron flux to the global ocean. Geophys. Res. Lett. 28, 29–32.

Gao, Y., Xu, G., Zhan, J., Zhang, J., Li, W., Lin, Q., Chen, L., Lin, H., 2013. Spatial and particle size distributions of atmospheric dissolvable iron in aerosols and its input to the Southern Ocean and coastal East Antarctica. J. Geophys. Res. Atmos. 118, 12634–12648. doi:10.1002/2013JD020367

Garibotti, I.A., Vernet, M., Smith, R.C., Ferrario, M.E., 2005. Interannual variability in the distribution of the phytoplankton standing stock across the seasonal sea-ice zone

west of the Antarctic Peninsula. J. Plankton Res. 27, 825–843. doi:10.1093/plankt/fbi056

Garibotti, I., Vernet, M., Ferrario, M., Smith, R., Ross, R., Quetin, L., 2003. Phytoplankton spatial distribution patterns along the western Antarctic Peninsula (Southern Ocean). Mar. Ecol. Prog. Ser. 261, 21–39. doi:10.3354/meps261021

Gerringa, L.J.A., Alderkamp, A.-C., Laan, P., Thuroczy, C.-E., de Baar, H.J.W., Mills, M.M., van Dijken, G.L., van Haren, H., Arrigo, K.R., 2012. Iron from melting glaciers fuels phytoplankton blooms in the Amundsen Sea (Southern Ocean): Iron biogeochemistry. Deep. Res. Part II Top. Stud. Oceanogr. 71–76, 16–31. doi:10.1016/j.dsr2.2012.03.007

Hansen, J., Ruedy, R., Glascoe, J., Sato, M., 1999. GISS analysis of surface temperature change. J. Geophys. Res. 104, 30997–31022.

Hatta, M., Measures, C.I., Selph, K.E., Zhou, M., Hiscock, W.T., 2013. Iron fluxes from the shelf regions near the South Shetland Islands in the Drake Passage during the austral-winter 2006. Deep. Res. Part II Top. Stud. Oceanogr. 90, 89–101. doi:10.1016/j.dsr2.2012.11.003

Hewes, C.D., Reiss, C.S., Kahru, M., Mitchell, B.G., Holm-Hansen, O., 2008. Control of phytoplankton biomass by dilution and mixed layer depth in the western Weddell-scotia confluence. Mar. Ecol. Prog. Ser. 366, 15–29. doi:10.3354/meps07515

Hofmann, E.E., Klinck, J.M., 1998. Hydrography and circulation of Antarctic Continental Shelf:150°E eastward to the Greenwich Meridian, in: Brink, K.H., Robinson, A.R. (Eds.), The Sea, The Global Coastal Ocean, Regional Studies and Synthesis Vol. 11. John Wiley & Sons, New York, pp. 997–1042.

Holm-Hansen, O., Kahru, M., Hewes, C.D., 2005. Deep chlorophyll a maxima (DCMs) in pelagic Antarctic waters. II. Relation to bathymetric features and dissolved iron concentrations. Mar. Ecol. Prog. Ser. 297, 71–81. doi:Doi 10.3354/Meps297071

Huang, K., Ducklow, H., Vernet, M., Cassar, N., Bender, M.L., 2012. Export production and its regulating factors in the West Antarctica Peninsula region of the Southern Ocean. Global Biogeochem. Cycles 26, 1–13. doi:10.1029/2010GB004028

Jenkins, A., Jacobs, S., 2008. Circulation and melting beneath George VI ice shelf, Antartica. J. Geophys. Res. Ocean. 113. doi:10.1029/2007JC004449

Jiang, M., Barbeau, K.A., Selph, K.E., Measures, C.I., Buck, K.N., Azam, F., Greg Mitchell, B., Zhou, M., 2013a. The role of organic ligands in iron cycling and primary productivity in the Antarctic Peninsula: A modeling study. Deep. Res. Part II Top. Stud. Oceanogr. 90, 112–133. doi:10.1016/j.dsr2.2013.01.029

Jiang, M., Charette, M.A., Measures, C.I., Zhu, Y., Zhou, M., 2013b. Seasonal cycle of circulation in the Antarctic Peninsula and the off-shelf transport of shelf waters into southern Drake Passage and Scotia Sea. Deep. Res. Part II Top. Stud. Oceanogr. 90, 15–30. doi:10.1016/j.dsr2.2013.02.029

Jickells, T.D., 2005. Global Iron Connections Between Desert Dust, Ocean Biogeochemistry, and Climate. Science (80-.). 308, 67–71. doi:10.1126/science.1105959

Kavanaugh, M.T., Abdala, F.N., Ducklow, H., Glover, D., Fraser, W., Martinson, D., Stammerjohn, S., Schofield, O., Doney, S.C., 2015. Effect of continental shelf canyons on phytoplankton biomass and community composition along the western Antarctic Peninsula. Mar. Ecol. Prog. Ser. 524, 11–26. doi:10.3354/meps11189

Kim, I., Kim, G., Choy, E.J., 2015. The significant inputs of trace elements and rare earth elements from melting glaciers in Antarctic coastal waters 1, 1–13.

Klinck, J.M., 1998. Heat and salt changes on the continental shelf west of the Antarctic Peninsula between January 1993 and January 1994. J. Geophys. Res. 103, 7617–7636. doi:10.1029/98JC00369

Klunder, M.B., Laan, P., De Baar, H.J.W., Middag, R., Neven, I., Van Ooijen, J., 2014. Dissolved Fe across the Weddell Sea and Drake Passage: Impact of DFe on nutrient uptake. Biogeosciences 11, 651–669. doi:10.5194/bg-11-651-2014

Kryc, K. a., Murray, R.W., Murray, D.W., 2003. Al-to-oxide and Ti-to-organic linkages in biogenic sediment: Relationships to paleo-export production and bulk Al/Ti. Earth Planet. Sci. Lett. 211, 125–141. doi:10.1016/S0012-821X(03)00136-5

Lagerström, M.E., Field, M.P., Séguret, M., Fischer, L., Hann, S., Sherrell, R.M., 2013. Automated on-line flow-injection ICP-MS determination of trace metals (Mn, Fe, Co, Ni, Cu and Zn) in open ocean seawater: Application to the GEOTRACES program. Mar. Chem. 155, 71–80. doi:10.1016/j.marchem.2013.06.001

Lannuzel, D., Bowie, A.R., van der Merwe, P.C., Townsend, A.T., Schoemann, V., 2011.

Distribution of dissolved and particulate metals in Antarctic sea ice. Mar. Chem. 124, 134–146. doi:10.1016/j.marchem.2011.01.004

Lannuzel, D., Schoemann, V., de Jong, J., Pasquer, B., van der Merwe, P., Masson, F., Tison, J.-L., Bowie, A., 2010. Distribution of dissolved iron in Antarctic sea ice: Spatial, seasonal, and inter-annual variability. J. Geophys. Res. 115, 1–13. doi:10.1029/2009JG001031

Lannuzel, D., Schoemann, V., de Jong, J., Tison, J.L., Chou, L., 2007. Distribution and biogeochemical behaviour of iron in the East Antarctic sea ice. Mar. Chem. 106, 18–32. doi:10.1016/j.marchem.2006.06.010

Lannuzel, D., Schoemann, V., Dumont, I., Content, M., de Jong, J., Tison, J.L., Delille, B., Becquevort, S., 2013. Effect of melting Antarctic sea ice on the fate of microbial communities studied in microcosms. Polar Biol. 36, 1483–1497. doi:10.1007/s00300-013-1368-7

Lannuzel, D., van der Merwe, P.C., Townsend, A.T., Bowie, A.R., 2014. Size fractionation of iron, manganese and aluminium in Antarctic fast ice reveals a lithogenic origin and low iron solubility. Mar. Chem. 161, 47–56. doi:10.1016/j.marchem.2014.02.006

Lin, H., Rauschenberg, S., Hexel, C.R., Shaw, T.J., Twining, B.S., 2011. Free-drifting icebergs as sources of iron to the Weddell Sea. Deep. Res. Part II Top. Stud. Oceanogr. 58, 1392–1406. doi:10.1016/j.dsr2.2010.11.020

Lis, H., Shaked, Y., Kranzler, C., Keren, N., Morel, F.M.M., 2014. Iron bioavailability to phytoplankton: an empirical approach. ISME J. 9, 1003–1013. doi:10.1038/ismej.2014.199

Martin, J., Fitzwater, S.E., Gordon, R.M., 1990. Iron deficiency limits phytoplankton growth in Antarctic waters. Global Biogeochem. Cycles 4, 5–12.

Martinson, D.G., McKee, D.C., 2012. Transport of warm upper circumpolar deep water onto the Western Antarctic Peninsula Continental Shelf. Ocean Sci. 8, 433–442. doi:10.5194/os-8-433-2012

Martinson, D.G., Stammerjohn, S.E., Iannuzzi, R.A., Smith, R.C., Vernet, M., 2008. Western Antarctic Peninsula physical oceanography and spatio–temporal variability. Deep Sea Res. Part II Top. Stud. Oceanogr. 55, 1964–1987.

doi:10.1016/j.dsr2.2008.04.038

McGillicuddy, D.J., Sedwick, P.N., Dinniman, M.S., Arrigo, K.R., Bibby, T.S., Greenan, B.J.W., Hofmann, E.E., Klinck, J.M., Smith, W.O., Mack, S.L., Marsay, C.M., Sohst, B.M., Van Dijken, G.L., 2015. Iron supply and demand in an Antarctic shelf ecosystem. Geophys. Res. Lett. 42, 8088–8097. doi:10.1002/2015GL065727

McLennan, S.., 2001. Relationships between the trace element composition of sedimentary rocks and upper continental crust. Geochemistry, Geophys. Geosystems 2, Paper number 2000GC000109.

Measures, C.I., Brown, M.T., Selph, K.E., Apprill, A., Zhou, M., Hatta, M., Hiscock, W.T., 2013. The influence of shelf processes in delivering dissolved iron to the HNLC waters of the Drake Passage, Antarctica. Deep. Res. Part II Top. Stud. Oceanogr. 90, 77–88. doi:10.1016/j.dsr2.2012.11.004

Meredith, M.P., Brandon, M.A., Wallace, M.I., Clarke, A., Leng, M.J., Renfrew, I.A., van Lipzig, N.P.M., King, J.C., 2008. Variability in the freshwater balance of northern Marguerite Bay, Antarctic Peninsula: Results from d18O. Deep. Res. Part II Top. Stud. Oceanogr. 55, 309–322. doi:10.1016/j.dsr2.2007.11.005

Meredith, M.P., Stammerjohn, S.E., Venables, H.J., Ducklow, H.W., Martinson, D.G., Iannuzzi, R.A., Leng, M.J., van Wessem, J.M., Reijmer, C.H., Barrand, N.E., 2016. Changing distributions of sea ice melt and meteoric water west of the Antarctic Peninsula. Deep Sea Res. Part II Top. Stud. Oceanogr. 1–18. doi:10.1016/j.dsr2.2016.04.019

Middag, R., De Baar, H.J.W., Laan, P., Cai, P.H., Van Ooijen, J.C., 2011. Dissolved manganese in the Atlantic sector of the Southern Ocean. Deep Sea Res. Part II Top. Stud. Oceanogr. 58, 2661–2677. doi:10.1016/S0967-0645(96)00064-1

Millero, F.J., Sotolongo, S., Izaguirre, M., 1987. The oxidation kinetics of Fe(II) in seawater. Geochim. Cosmochim. Acta 51, 793–801. doi:10.1016/0016-7037(87)90093-7

Moffat, C., Beardsley, R.C., Owens, B., van Lipzig, N., 2008. A first description of the Antarctic Peninsula Coastal Current. Deep. Res. Part II Top. Stud. Oceanogr. 55, 277–293. doi:10.1016/j.dsr2.2007.10.003

Moffat, C., Owens, B., Beardsley, R.C., 2009. On the characteristics of Circumpolar

Deep Water intrusions to the west Antarctic Peninsula Continental Shelf. J. Geophys. Res. Ocean. 114. doi:10.1029/2008JC004955

Montes-Hugo, M., Martinson, D., Stammerjohn, S.E., Schofield, O., 2009. Recent Changes in Phytoplankton Western Antarctic Peninsula. Science (80-.). 323, 1470–1473.

Moreau, S., Mostajir, B., Belanger, S., Schloss, I.R., Vancoppenolle, M., Demers, S., Ferreyra, G.A., 2015. Climate change enhances primary production in the western Antarctic Peninsula. Glob. Chang. Biol. 21, 2191–2205. doi:10.1111/gcb.12878

Noble, A.E., Lamborg, C.H., Ohnemus, D.C., Lam, P.J., Goepfert, T.J., Measures, C.I., Frame, C.H., Casciotti, K.L., Ditullio, G.R., Jennings, J., 2012. Basin-scale inputs of cobalt , iron , and manganese from the Benguela-Angola front to the South Atlantic Ocean. Limnol. Oceanogr. 57, 989–1010. doi:10.4319/lo.2012.57.4.0989

Pakhomova, S. V., Hall, P.O.J., Kononets, M.Y., Rozanov, A.G., Tengberg, A., Vershinin, A. V., 2007. Fluxes of iron and manganese across the sediment-water interface under various redox conditions. Mar. Chem. 107, 319–331. doi:10.1016/j.marchem.2007.06.001

Parkinson, C.L., Cavalieri, D.J., 2012. Antarctic sea ice variability and trends, 1979-2010. Cryosphere 6, 871–880. doi:10.5194/tc-6-871-2012

Planquette, H., Sherrell, R.M., 2012. Sampling for particulate trace element determination using water sampling bottles: methodology and comparison to in situ pumps. Limnol. Oceanogr. Methods 10, 367–388. doi:10.4319/lom.2012.10.367

Planquette, H., Sherrell, R.M., Stammerjohn, S., Field, M.P., 2013. Particulate iron delivery to the water column of the Amundsen Sea, Antarctica. Mar. Chem. 153, 15–30. doi:10.1016/j.marchem.2013.04.006

Potter, J.R., Talbot, M.H., Paren, J.G., 1988. Oceanic regimes at the ice fronts of George VI Sound, Antarctic Peninsula. Cont. Shelf Res. 8, 347–362. doi:10.1016/0278-4343(88)90008-8

Prézelin, B.B., Hofmann, E.E., Moline, M., Klinck, J.M., 2004. Physical Forcing of Phytoplankton Community Structure and Primary Production in Continental Shelf Waters of the Western Antarctic Peninsula. J. Mar. Res. 62, 419–460. doi:10.1357/0022240041446173

Pritchard, H.D., Vaughan, D.G., 2007. Widespread acceleration of tidewater glaciers on the Antarctic Peninsula. J. Geophys. Res. Earth Surf. 112. doi:10.1029/2006JF000597

Raiswell, R., Benning, L.G., Tranter, M., Tulaczyk, S., 2008. Bioavailable iron in the Southern Ocean: the significance of the iceberg conveyor belt. Geochem. Trans. 9, 7. doi:10.1186/1467-4866-9-7

Raiswell, R., Hawkings, J.R., Benning, L.G., Baker, A.R., Death, R., Albani, S., Mahowald, N., Krom, M.D., Poulton, S.W., Wadham, J., Tranter, M., 2016. Potentially Bioavailable Iron Delivery by Iceberg-hosted Sediments and Atmospheric Dust to the Polar Oceans. Biogeosciences 13, 3887–3900. doi:10.5194/bg-2016-20

Ross, R.M., Quetin, L.B., Lascara, C., 1996. Distribution of Antarctic krill and dominant zooplankton west of the Antarctic Peninsula. Found. Ecol. Res. west Antarct. Penins. 70, 199–217.

Saba, G.K., Fraser, W.R., Saba, V.S., Iannuzzi, R. a, Coleman, K.E., Doney, S.C., Ducklow, H.W., Martinson, D.G., Miles, T.N., Patterson-Fraser, D.L., Stammerjohn, S.E., Steinberg, D.K., Schofield, O.M., 2014. Winter and spring controls on the summer food web of the coastal West Antarctic Peninsula. Nat. Commun. 5, 4318. doi:10.1038/ncomms5318

Sañudo-Wilhelmy, S.A., Olsen, K.A., Scelfo, J.M., Foster, T.D., Flegal, A.R., 2002. Trace metal distributions off the antarctic peninsula in the weddell sea. Mar. Chem. 77, 157–170. doi:10.1016/S0304-4203(01)00084-6

Savidge, D.K., Amft, J.A., 2009. Circulation on the West Antarctic Peninsula derived from 6 years of shipboard ADCP transects. Deep. Res. Part I Oceanogr. Res. Pap. 56, 1633–1655. doi:10.1016/j.dsr.2009.05.011

Schallenberg, C., Lannuzel, D., 2015. Dissolved iron and iron (II) distributions beneath the pack ice in the East Antarctic (120°E) during the winter/spring transition. Deep Sea Res. Part II Top. Stud. Oceanogr. doi:10.1016/j.dsr2.2015.02.019

Schmidtko, S., Heywood, K.J., Thompson, A.F., Aoki, S., 2014. Multidecadal warming of Antarctic waters. Sci. 346, 1227–1231. doi:10.1126/science.1256117

Shaked, Y., Lis, H., 2012. Disassembling iron availability to phytoplankton. Front.

Microbiol. 3, 1–26. doi:10.3389/fmicb.2012.00123

Sherrell, R.M., Lagerström, M.E., Forsch, K.O., Stammerjohn, S.E., Yager, P.L., 2015. Dynamics of dissolved iron and other bioactive trace metals (Mn, Ni, Cu, Zn) in the Amundsen Sea Polynya, Antarctica. Elem. Sci. Anthr. 3, 71. doi:10.12952/journal.elementa.000071

Smith, R.C., Martinson, D.G., Stammerjohn, S.E., Iannuzzi, R.A., Ireson, K., 2008. Bellingshausen and western Antarctic Peninsula region: Pigment biomass and sea-ice spatial/temporal distributions and interannual variabilty. Deep. Res. Part II Top. Stud. Oceanogr. 55, 1949–1963. doi:10.1016/j.dsr2.2008.04.027

Smith, W.O., Nelson, D.M., 1985. Phytoplankton Bloom Produced by a Receding Ice Edge in the Ross Sea: Spatial Coherence with the Density Field. Science (80-.). 163–166.

Spolaor, A., Vallelonga, P., Cozzi, G., Gabrieli, J., Varin, C., Kehrwald, N., Zennaro, P., Boutron, C., Barbante, C., 2013. Iron speciation in aerosol dust influences iron bioavailability over glacial-interglacial timescales. Geophys. Res. Lett. 40, 1618–1623. doi:10.1002/grl.50296

Stammerjohn, S., Massom, R., Rind, D., Martinson, D., 2012. Regions of rapid sea ice change: An inter-hemispheric seasonal comparison. Geophys. Res. Lett. 39, 1–8. doi:10.1029/2012GL050874

Stammerjohn, S.E., Martinson, D.G., Smith, R.C., Iannuzzi, R.A., 2008. Sea ice in the western Antarctic Peninsula region: Spatio-temporal variability from ecological and climate change perspectives. Deep. Res. Part II Top. Stud. Oceanogr. 55, 2041–2058. doi:10.1016/j.dsr2.2008.04.026

Steinberg, D.K., Ruck, K.E., Gleiber, M.R., Garzio, L.M., Cope, J.S., Bernard, K.S., Stammerjohn, S.E., Schofield, O.M.E., Quetin, L.B., Ross, R.M., 2015. Long-term (1993-2013) changes in macrozooplankton off the western antarctic peninsula. Deep. Res. Part I Oceanogr. Res. Pap. 101, 54–70. doi:10.1016/j.dsr.2015.02.009

Tagliabue, A., Bopp, L., Aumont, O., 2009. Evaluating the importance of atmospheric and sedimentary iron sources to Southern Ocean biogeochemistry. Geophys. Res. Lett. 36, 1–5. doi:10.1029/2009GL038914

Tagliabue, A., Bowie, A.R., Philip, W., Buck, K.N., Johnson, K.S., Saito, M.A., 2017.

The integral role of iron in ocean biogeochemistry. Nature 543, In Press. doi:10.1038/nature21058

Tagliabue, A., Sallée, J.-B., Bowie, A.R., Lévy, M., Swart, S., Boyd, P.W., 2014. Surface-water iron supplies in the Southern Ocean sustained by deep winter mixing. Nat. Geosci. 7, 314–320. doi:10.1038/NGEO2101

Taylor, S.., McLennan, S.., 1995. The geochemical evolution of the continental crust. Rev. Geophys. 33, 241–265. doi:10.1029/95RG00262

Thuróczy, C.E., Alderkamp, A.C., Laan, P., Gerringa, L.J.A., Mills, M.M., Van Dijken, G.L., De Baar, H.J.W., Arrigo, K.R., 2012. Key role of organic complexation of iron in sustaining phytoplankton blooms in the Pine Island and Amundsen Polynyas (Southern Ocean). Deep. Res. Part II Top. Stud. Oceanogr. 71–76, 49–60. doi:10.1016/j.dsr2.2012.03.009

van der Merwe, P., Lannuzel, D., Bowie, A.R., Mancuso Nichols, C.A., Meiners, K.M., 2011. Iron fractionation in pack and fast ice in East Antarctica: Temporal decoupling between the release of dissolved and particulate iron during spring melt. Deep. Res. Part II Top. Stud. Oceanogr. 58, 1222–1236. doi:10.1016/j.dsr2.2010.10.036

Van Der Merwe, P., Lannuzel, D., Bowie, A.R., Meiners, K.M., 2011. High temporal resolution observations of spring fast ice melt and seawater iron enrichment in East Antarctica. J. Geophys. Res. Biogeosciences 116, 1–18. doi:10.1029/2010JG001628

Venables, H.J., Clarke, A., Meredith, M.P., 2013. Wintertime controls on summer stratification and productivity at the western Antarctic Peninsula. Limnol. Oceanogr. 58, 1035–1047. doi:10.4319/lo.2013.58.3.1035

Venables, H.J., Meredith, M.P., Brearley, J.A., 2016. Modification of deep waters in Marguerite Bay, western Antarctic Peninsula, caused by topographic overflows. Deep Sea Res. Part II Top. Stud. Oceanogr. in press.

Vernet, M., Martinson, D., Iannuzzi, R., Stammerjohn, S., Kozlowski, W., Sines, K., Smith, R., Garibotti, I., 2008. Primary production within the sea-ice zone west of the Antarctic Peninsula: I-Sea ice, summer mixed layer, and irradiance. Deep. Res. Part II Top. Stud. Oceanogr. 55, 2068–2085. doi:10.1016/j.dsr2.2008.05.021

Wadham, J.L., De'ath, R., Monteiro, F.M., Tranter, M., Ridgwell, a., Raiswell, R., Tulaczyk, S., 2013. The potential role of the Antarctic Ice Sheet in global

biogeochemical cycles. Earth Environ. Sci. Trans. R. Soc. Edinburgh 104, 55–67. doi:10.1017/S1755691013000108

Wagener, T., Guieu, C., Losno, R., Bonnet, S., Mahowald, N., 2008. Revisiting atmospheric dust export to the Southern Hemisphere ocean: Biogeochemical implications. Global Biogeochem. Cycles 22, 1–13. doi:10.1029/2007GB002984

Weston, K., Jickells, T.D., Carson, D.S., Clarke, A., Meredith, M.P., Brandon, M.A., Wallace, M.I., Ussher, S.J., Hendry, K.R., 2013. Primary production export flux in Marguerite Bay (Antarctic Peninsula): Linking upper water-column production to sediment trap flux. Deep. Res. Part I Oceanogr. Res. Pap. 75, 52–66. doi:10.1016/j.dsr.2013.02.001

Winton, V.H.L., Bowie, A.R., Edwards, R., Keywood, M., Townsend, A.T., van der Merwe, P., Bollhöfer, A., 2015. Fractional iron solubility of atmospheric iron inputs to the Southern Ocean. Mar. Chem. 177, 20–32. doi:10.1016/j.marchem.2015.06.006

Zhou, M., Zhu, Y., Measures, C.I., Hatta, M., Charette, M.A., Gille, S.T., Frants, M., Jiang, M., Greg Mitchell, B., 2013. Winter mesoscale circulation on the shelf slope region of the southern Drake Passage. Deep. Res. Part II Top. Stud. Oceanogr. 90, 4–14. doi:10.1016/j.dsr2.2013.03.041

7. Tables

Table 1: Results of multiple analyses of seawater trace metal reference materials. Solutions analyzed were SAFe (S and D2) and GEOTRACES (GS and GD), all results are presented in nmol kg^{-1}. Values have been presented in Lagerstrom et al. 2013, as analyses of samples presented here spanned the same date range. Consensus values from the May 2013 data compilation (http://www.geotraces.org/science/intercalibration/322-standards-and-reference-materials).

	SAFe S			**SAFe D2**		
	Determined	n	Consensus	Determined	n	Consensus
Fe	0.080 ± 0.018	62	0.093 ± 0.008	0.919 ± 0.049	41	0.933 ± 0.023
Mn	0.71 ± 0.04	54	0.79 ± 0.06	0.33 ± 0.03	36	0.35 ± 0.06
	GS			**GD**		
	Determined	n	Consensus	Determined	n	Consensus
Fe	0.588 ± 0.031	40	0.546 ± 0.046	1.06 ± 0.04	23	1.00 ± 0.10
Mn	1.30 ± 0.11	32	1.50 ± 0.11	0.20 ± 0.02	23	0.21 ± 0.03

Table 2: Dissolved trace metal concentrations in glacial meltwater collected near Palmer Station (Anvers Island), in January 2015 (full details in Methods section). Replicate samples collected within minutes. Units are nmol kg^{-1}.

Metal:	**Fe**	**Mn**
Replicate1	325.1	23.01
Replicate 2	353.9	36.56
Mean	**339.5**	**29.79**
Difference about mean	**4.2%**	**22.7%**

Table 3: Regressions of dFe and pFe versus % meteoric component (with respect to mean winter mixed layer) for 5 sampling lines in 2011, and extrapolated pure meteoric endmember concentrations. (*) values are from a regression forced by a single high concentration sample. ($^{@}$) does not include the 200-line estimate.

Line	dFe			pFe			Inferred meteoric water	
	Slope (pmol kg^{-1} /%met)	y-intercept (pmol kg^{-1})	r^2	Slope (pmol kg^{-1} /%met)	y-intercept (pmol kg^{-1})	r^2	dFe (nmol kg^{-1})	pFe (nmol kg^{-1})
-100	260	29	0.84	670	-19	0.96	26	67
100	3020	380	0.99	1350	560	0.96	300	140
200	450	72	0.73	20300*	-8900*	0.72*	45	2020
300	110	93	0.84	820	1050	0.56	11	83
400	74	46	0.48	1820	-3700	0.47	7.4	180
500	74	59	0.03	1680	-3400	0.14	7.3	164
600	560	170	0.70	3700	320	0.79	56	370
						MEAN:	64	112$^{@}$
						SD:	105	58$^{@}$

8. Figures and captions

Figure 1: The study area above the shelf of the western Antarctic Peninsula. White dots show typical station locations on the Palmer-LTER grid and geographic features discussed in the text. Surface water samples for trace metals reported here were collected along the white lines while underway. Red dot shows the location of Palmer Research Station. Adjacent black circle shows the location of Palmer Deep, a depression with a maximum depth of ~1400 m, at the location of sampling station 600.040. Contour line is drawn along the 500m isobath.

Figure 2: Temperature (top) and salinity (bottom) distributions in at sampling locations in surface waters, for all three study years. Sampling line numbers are labeled on bottom plots.

Figure 3: Percent contributions of sea ice melt (top) and meteoric water (bottom; = glacial and precipitation) in 2011 and 2012. Values are calculated with respect to the mean winter mixed layer (WML). Data from Meredith et al. 2016. Top right panel redrawn from Meredith et al. 2013. Sampling line numbers are labeled on bottom plots.

Figure 4: Dissolved (top) and particulate (bottom) Fe concentrations throughout the Pal-LTER sampling grid, for years 2010-2012 (sampling in January). Note that the maximum concentrations in 2011 extend beyond the color bars to 7.8 nM (dFe) and 42 nM (pFe; values shown in Supplementary Material Fig. S1). Contour lines are drawn at 0.15 nM for dFe, and 0.2 nM for pFe. White symbols show where pFe values were close to blank values (< mean plus 2 standard deviations of the filter blank). Sampling lines are labeled on bottom plots. Dotted line shows the location of the 500 m isobath along the shelf break and Marguerite Trough (smaller depressions on the shelf are not shown).

Figure 5: Dissolved and particulate Mn concentrations for January 2010 – 2012. Sampling lines are labeled on bottom plots. Dotted line shows the location of the 500 m isobath along the shelf break and Marguerite Trough (smaller depressions on the shelf are not shown).

Figure 6: Distribution of predominantly lithogenic particulate metals and metal ratios. Particulate Al (top), particulate Fe:Al (second row), Fe:Ti (third row) and Al:Ti (bottom). Years 2010 to 2012 are shown left to right, sampling lines are labeled on top plots. Color scales for ratios are set to white at average upper crustal values (McLennan, 2001), denoted by white triangles.

Figure 7: Iron and Mn concentrations versus salinity and meltwater for 2011. Dissolved Fe (a), particulate Fe (b) and dissolved Mn (c) versus salinity along all sampling lines. d, e and f: Dissolved Fe (dFe; left axis) and particulate Fe (pFe; right axis) versus sea ice (d) and meteoric water (e) contributions with respect to the winter mixed layer, and dissolved and particulate Mn (both on left axis) versus meteoric water (f) contributions, for the -100 sampling line only. (g, h and i): As for (d, e, f), but for the +100 sampling line only. (j, k and l): As for (d, e, f), but for the 200 sampling line only. Least-squares regression lines are shown where they are statistically significant ($p < 0.05$). Open symbols in (e, f) were not included in the regression (see text).

Figure 8: Spatial distribution of Mn:Fe ratios. Dissolved Mn:Fe (left) and particulate Mn:Fe (right) throughout the sampling grid in 2011, with 500 m isobaths contour in black. White triangles show average upper crustal values (from McLennan, 2001).

Figure 9: Spatial averages of Mn distributions. Top panels show average dMn (a) and dMn:dFe (b) for each sampling line, 2011. Bottom panels show dMn versus distance from nearest coast for 2011 (c) and 2012 (d). Error bars denote standard deviation, numbers on bars are the number of samples pooled per category.

Figure 10: Dissolved Fe and Mn versus distance from the nearest coast for the northern grid region. Dissolved Mn (left) and dFe (right) for the 400-600 sampling lines in 2012 Regressions for dMn (all points) and inshore dFe (<40 km from the nearest coast) are statistically significant ($p < 0.05$).

Figure 11: Mn and Fe distributions and elemental ratios in 2011 in relation to the shelf break. Dissolved and particulate Mn on the -100 line (a), dissolved and particulate Fe on the -100 line (b), and dissolved and particulate Mn:Fe on the -100 line (c). Shaded regions show the ~50 km region above the 500 m isobath. Distance is relative to nearest coastline.

Supplementary info:

S1. Variability in coastal particulate Fe

On the southernmost -100 sampling line in 2011 there were multiple coastal samples with similar contributions of ~1.75 % meteoric water, but varying pFe concentrations (Fig. 7e). This suggests that for these samples, either the pFe content of meteoric water is highly variable, pFe is variably non-conservative after input with meltwater, meteoric input is not a primary control on pFe, or all three. As these samples were collected nearest the shore, the non-linear relationship may be due to particles that sink rapidly near the coast, initially decoupling pFe from the meteoric component in a water parcel. As such, we have excluded these high pFe samples from the overall -100-line regression (in Table 3), as they are likely influenced by variable concentrations of fast-sinking large particles. Samples further away from the coast would thus reflect smaller, persistent particulate phases with slower sinking speeds that can be transported more conservatively offshore, reflected in the strong linear relationship away from shore (Table 3).

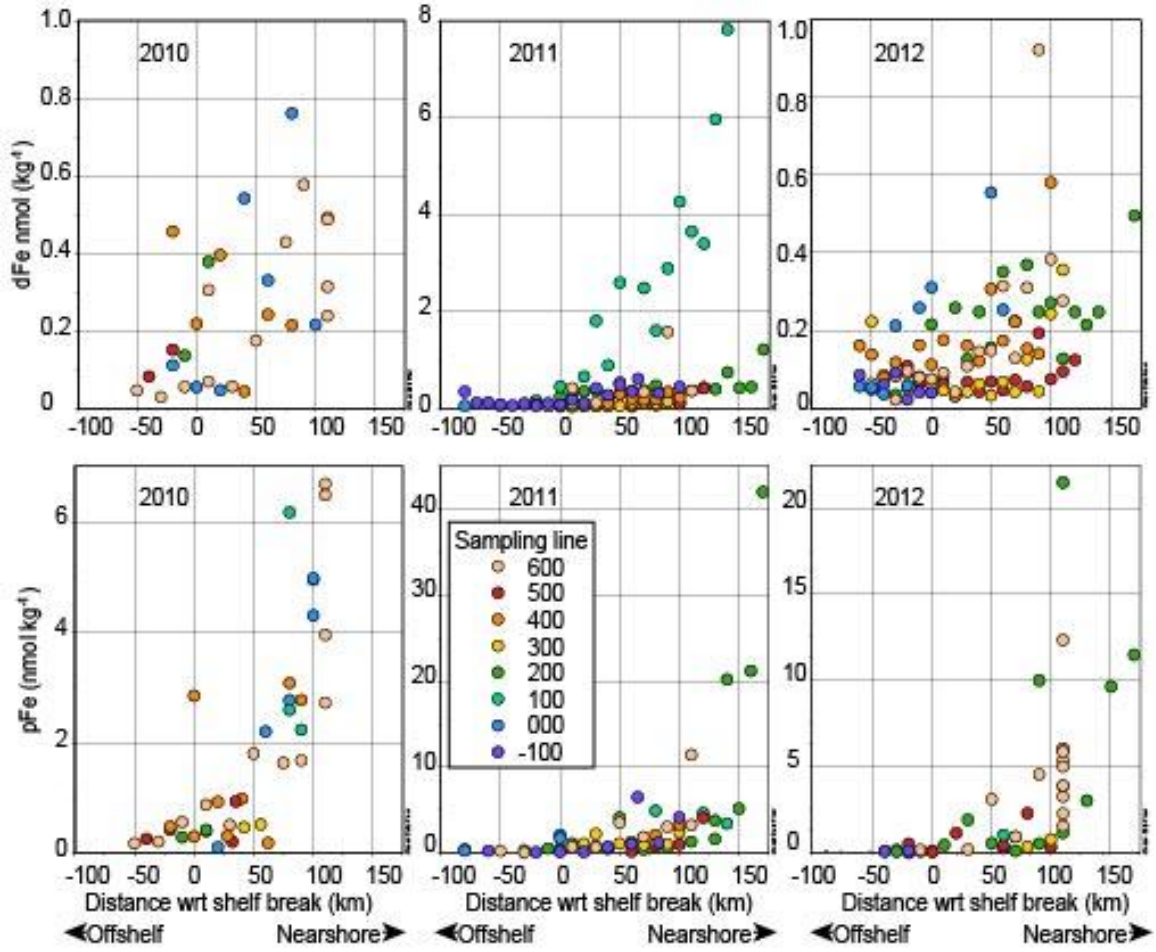

Figure S1: Dissolved and particulate Fe concentrations throughout the sampling region in each study year. Distances are given relative to the shelf break (500 m isobath), with positive values indicating the inshore direction and negative values denoting off-shelf samples.

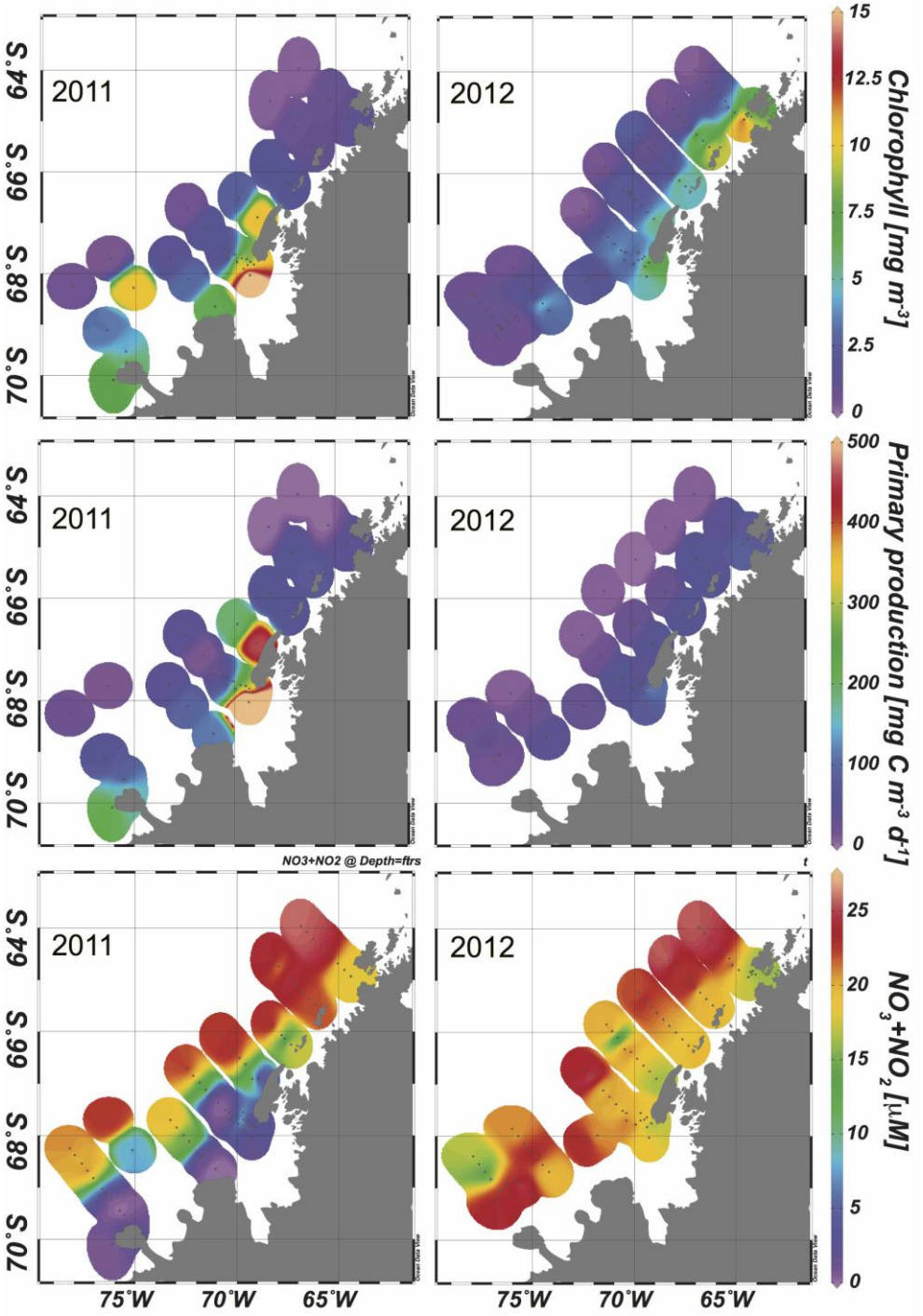

Figure S2: Comparison of proxies for biological Fe drawdown between 2011 (left) and 2012 (right). Shown are chlorophyll (top), primary productivity (middle), and dissolved inorganic N (NO_3^-+NO_2^-). All values are from surface water (0-10 m) from both CTD/rosette and underway sample collection. Data available from the Pal-LTER DataZoo: (http://oceaninformatics.ucsd.edu/datazoo/data/pallter/datasets).

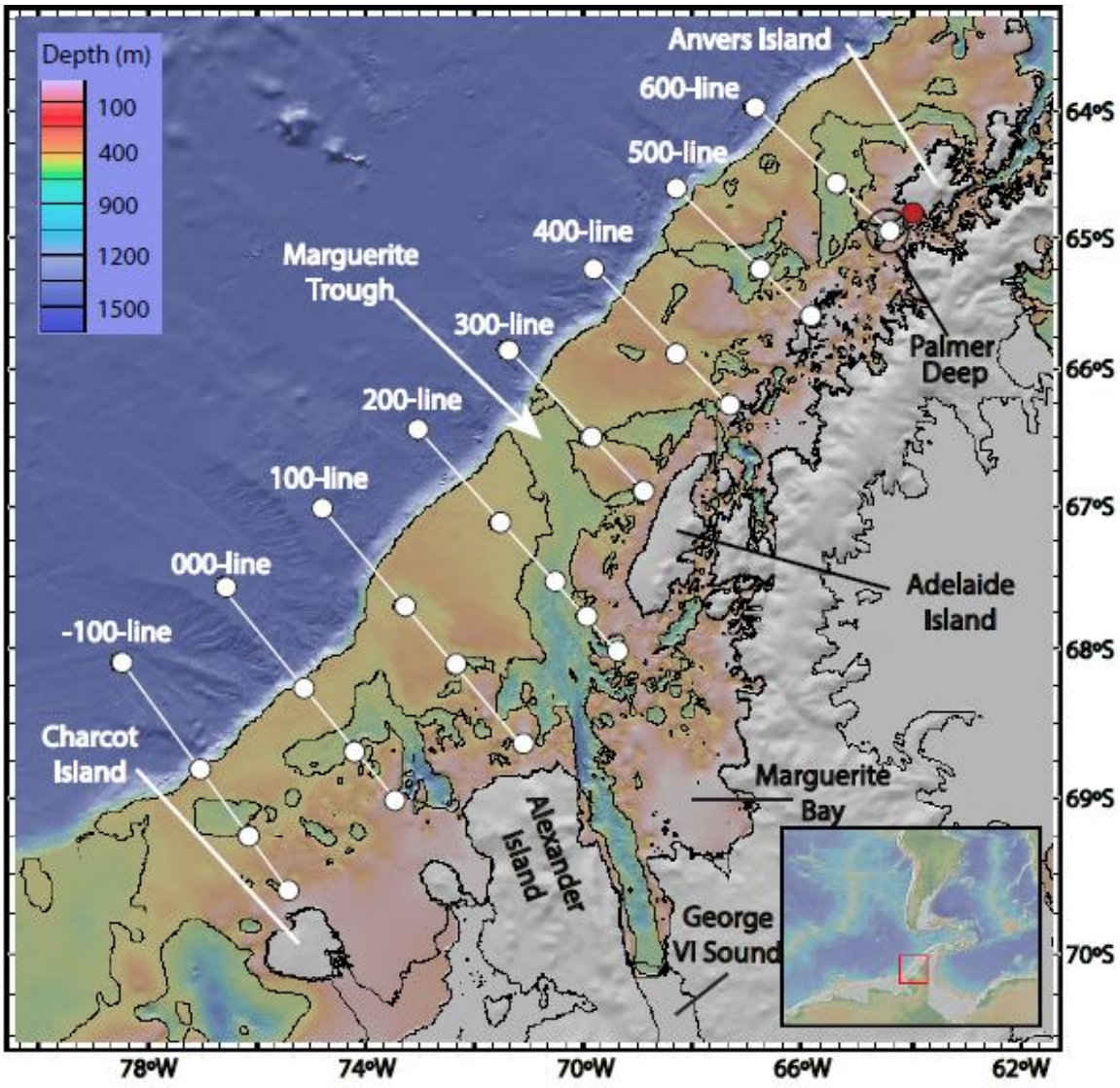

Fig. 1

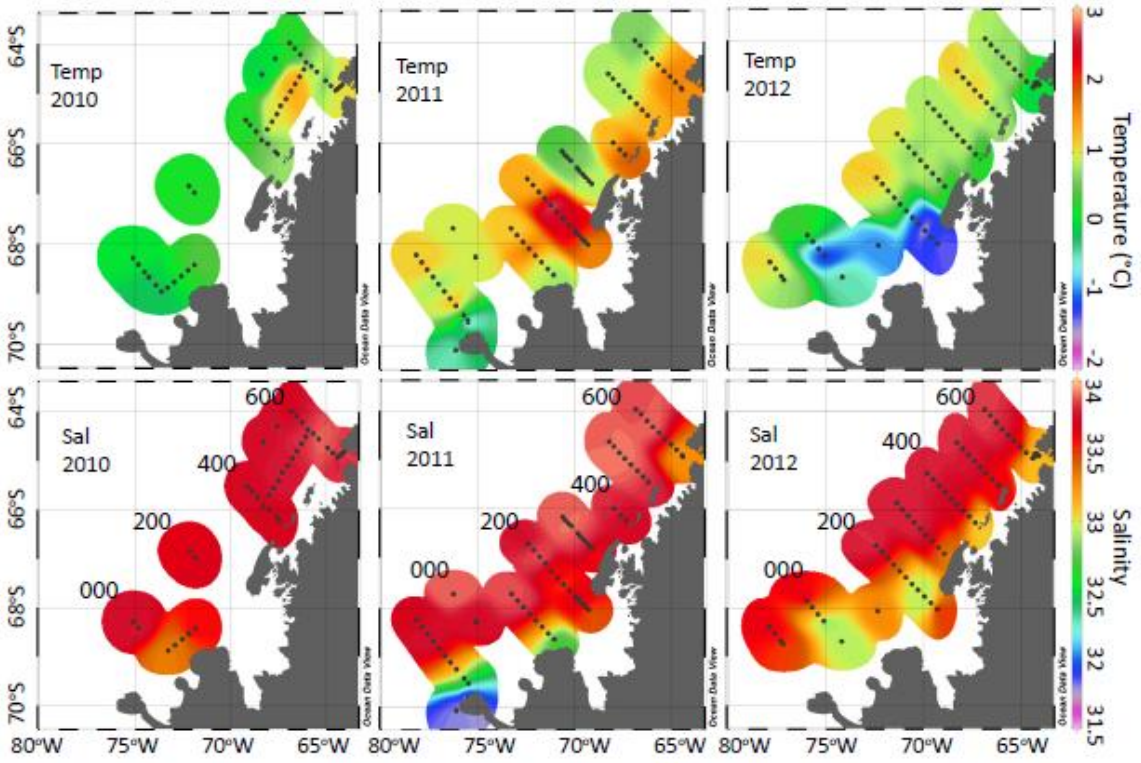

Fig. 2

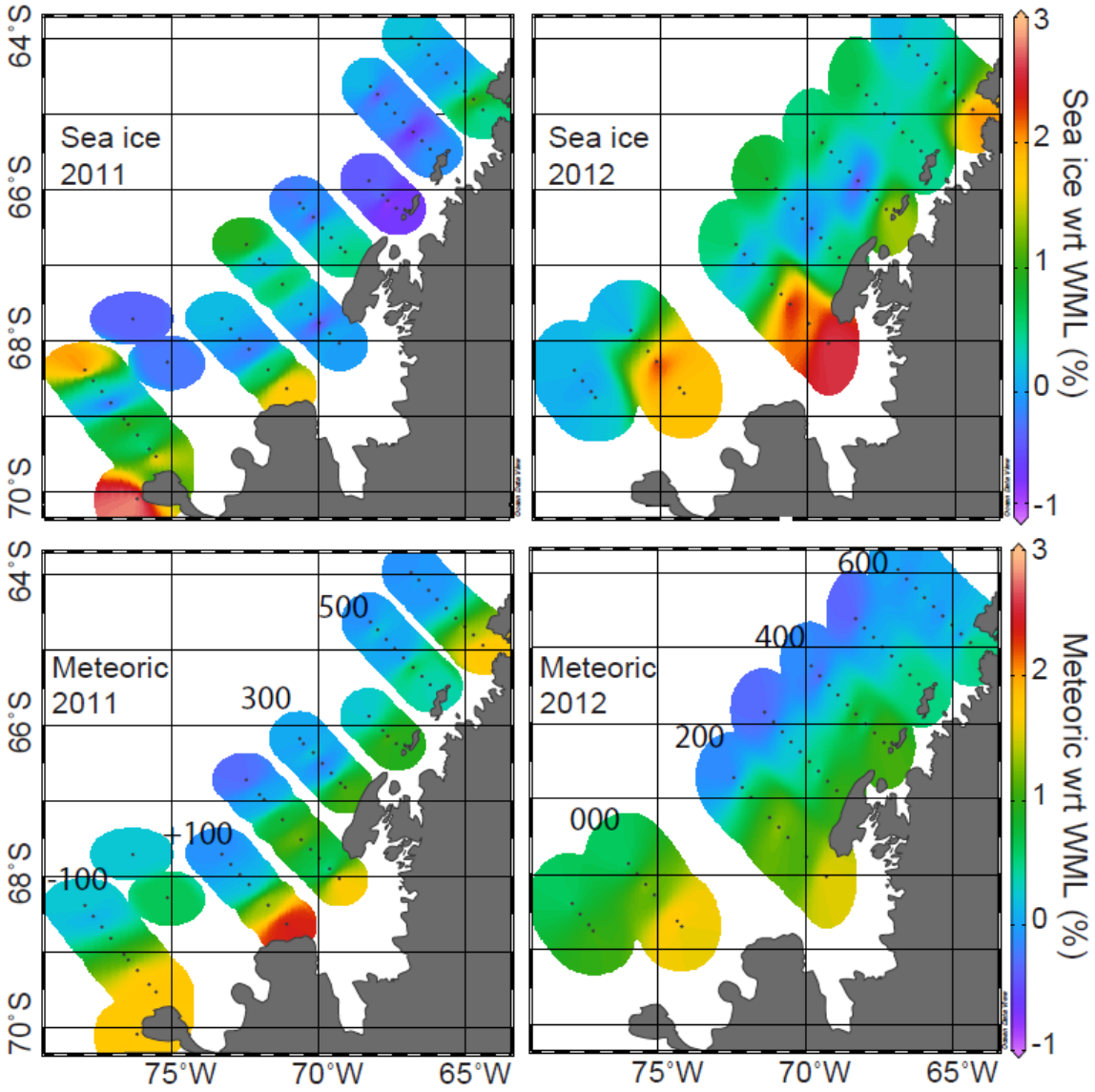

Fig. 3

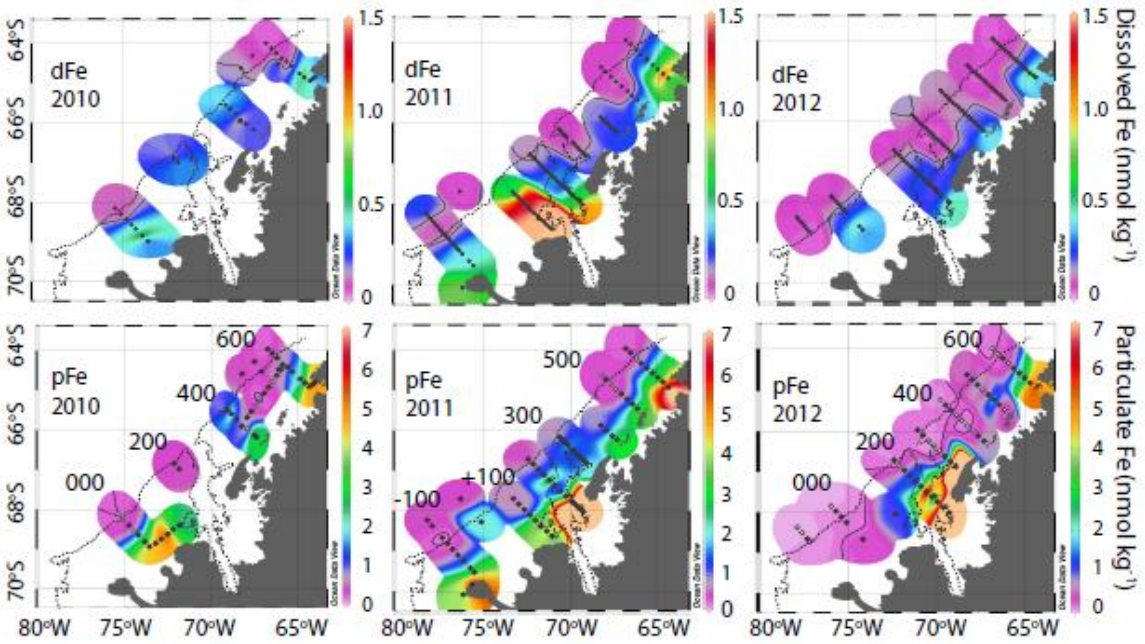

Fig. 4

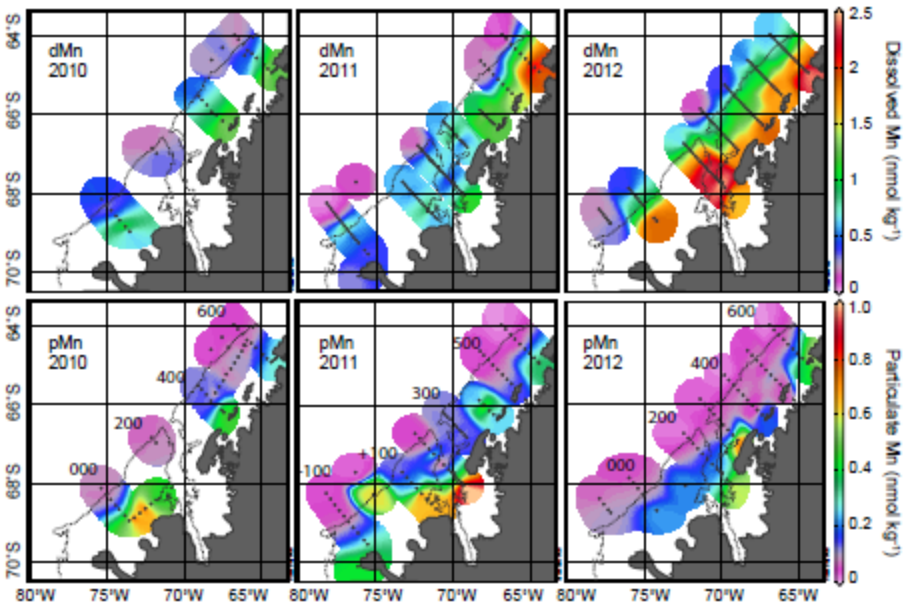

Fig. 5

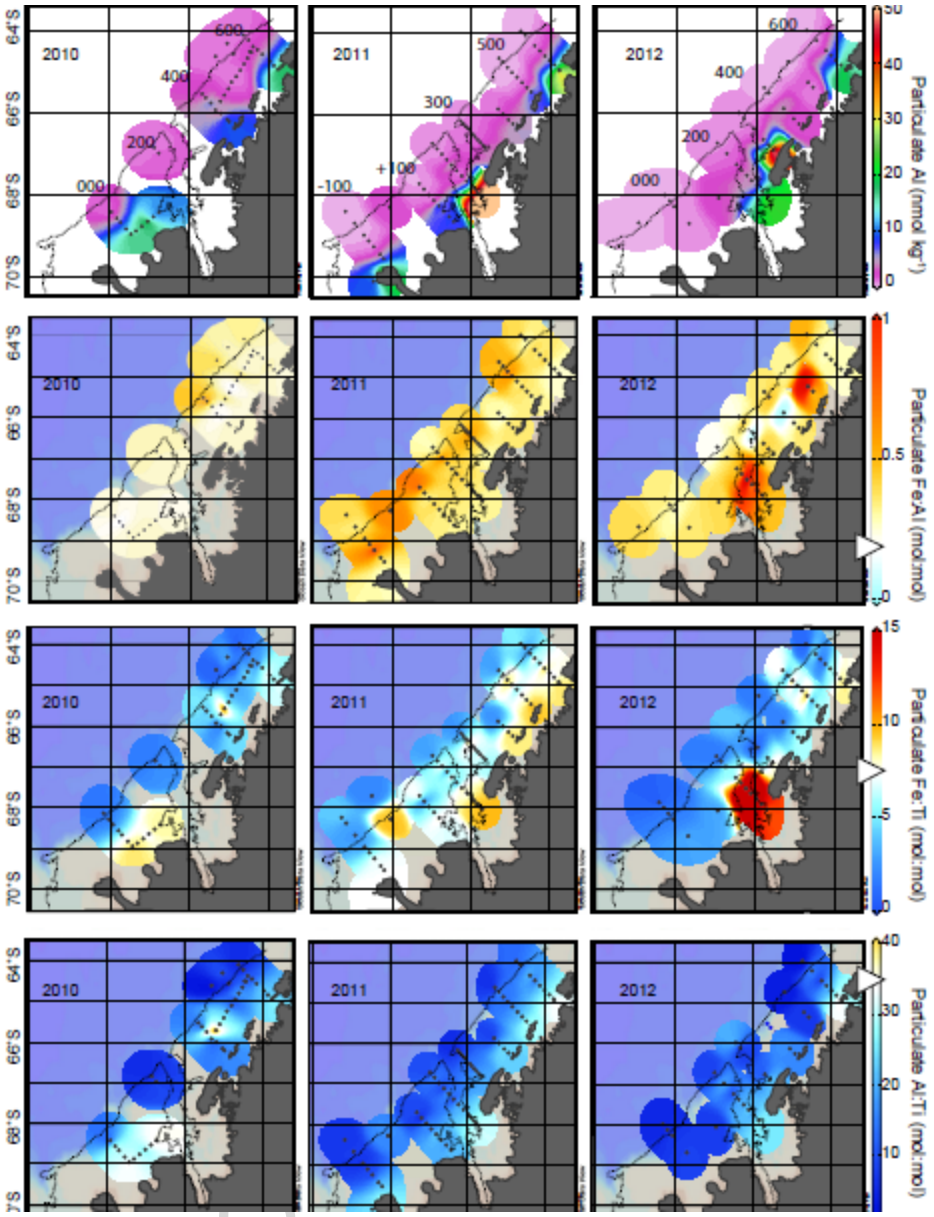

Fig. 6

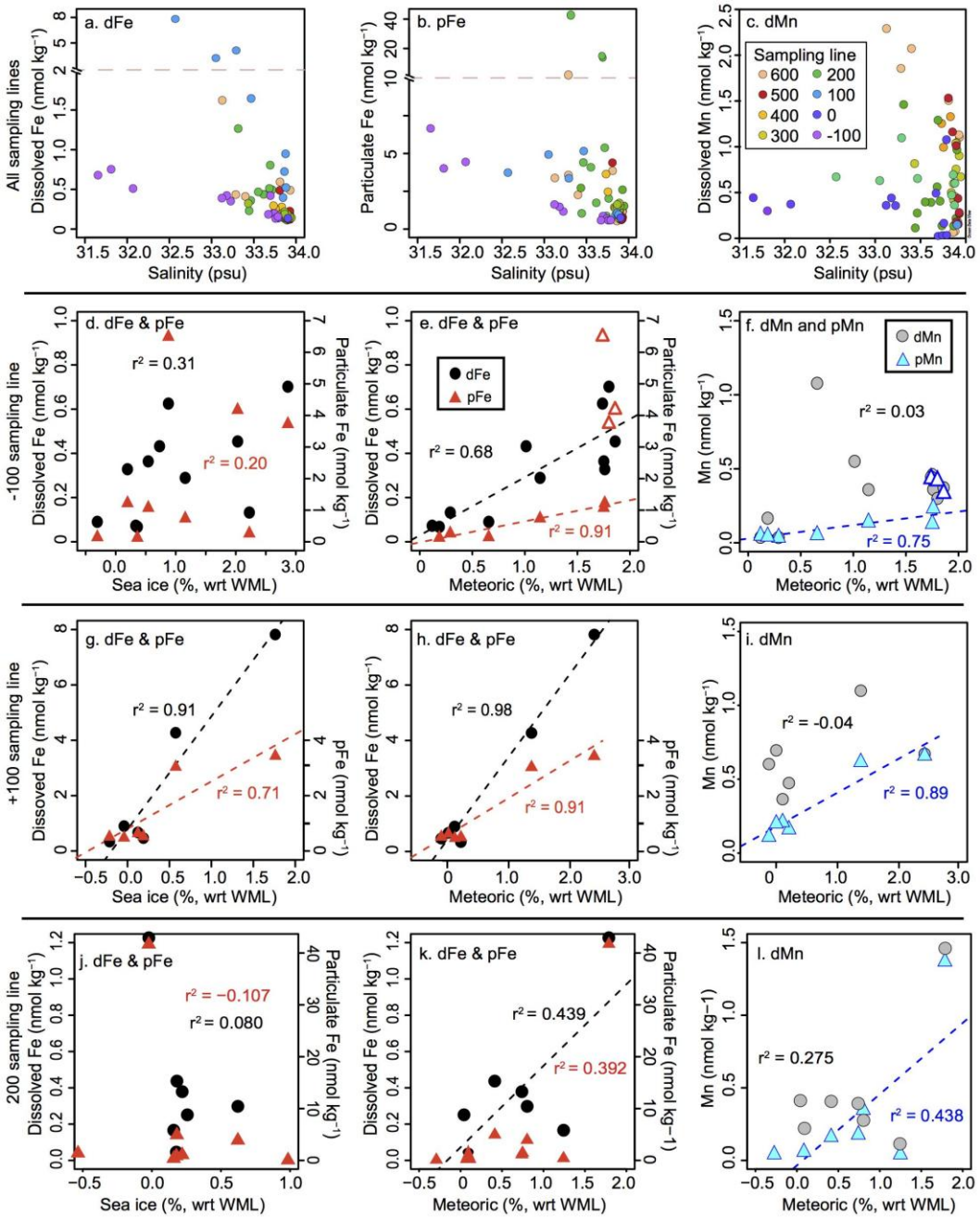

Fig. 7

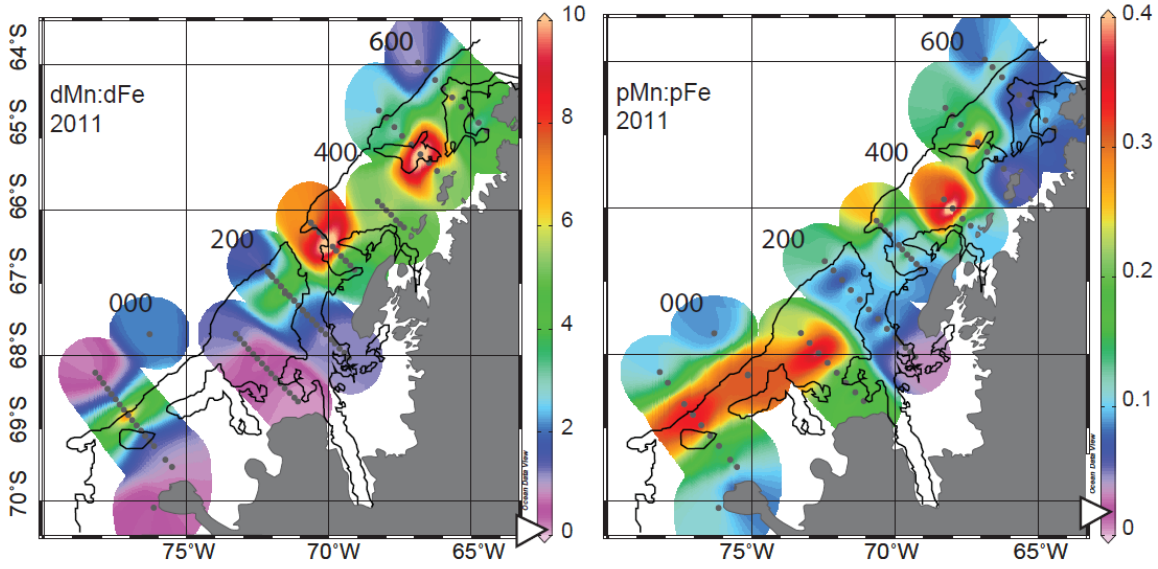

Fig. 8

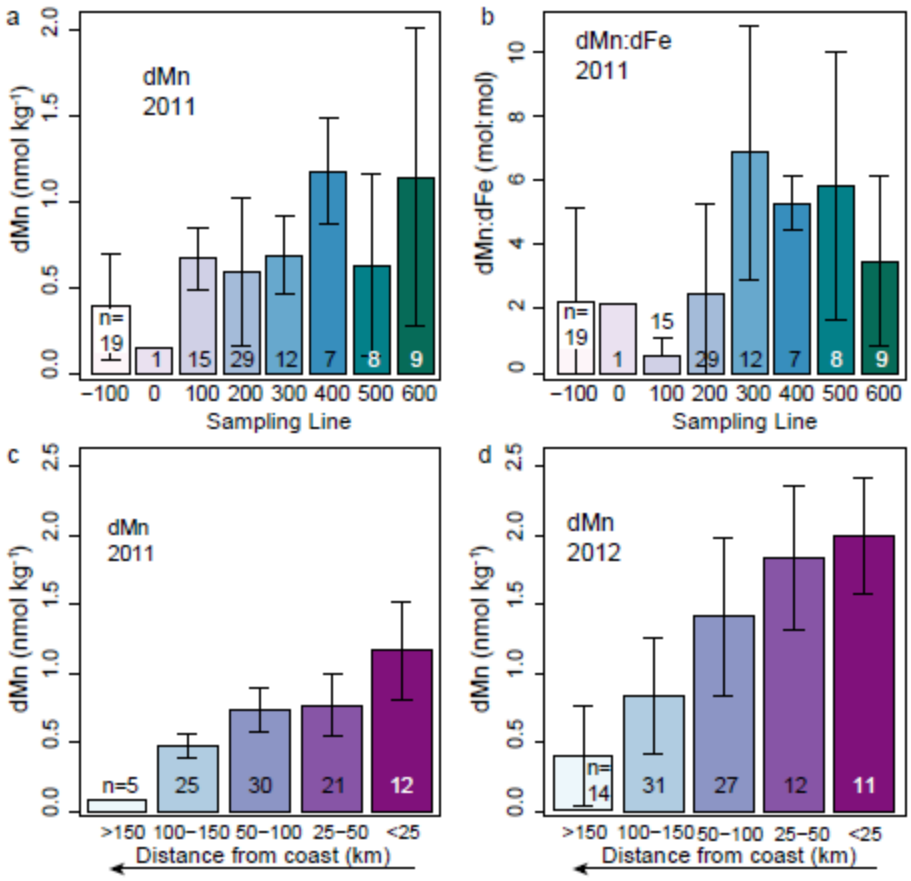

Fig. 9

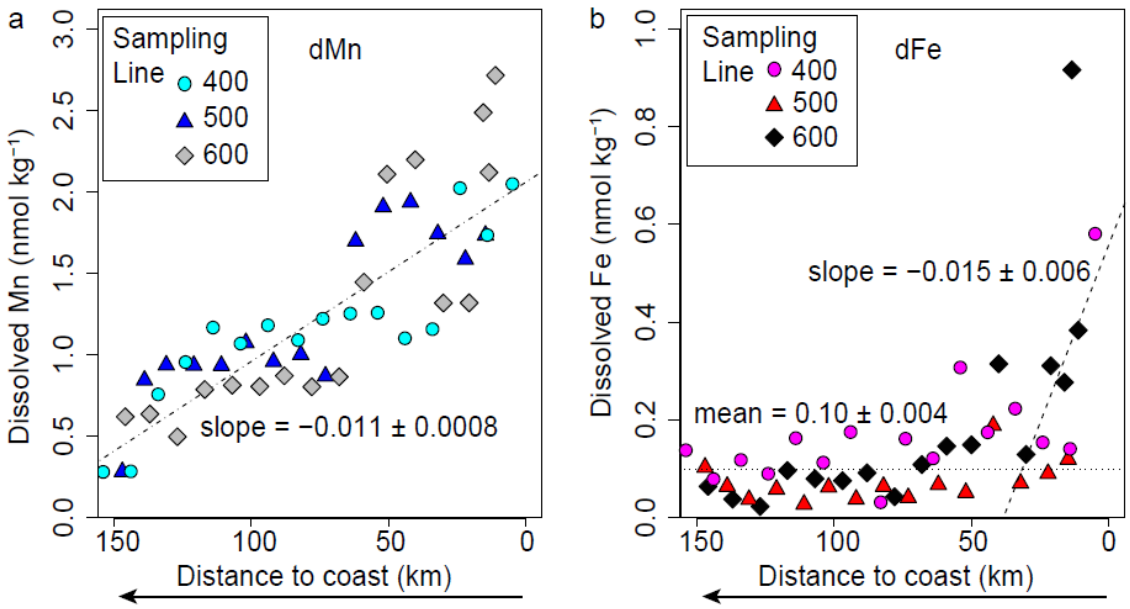

Fig. 10

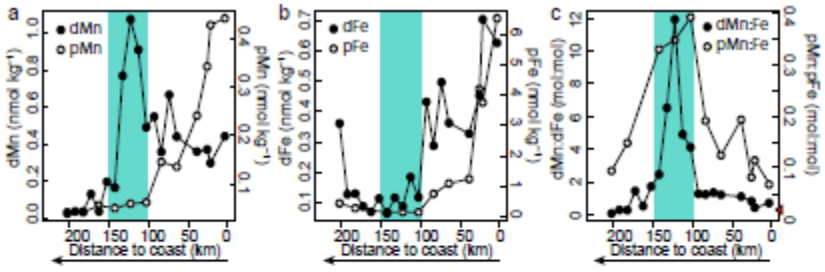

Fig. 11

Highlights: Controls on dissolved and particulate iron distributions in surface waters of the Western Antarctic Peninsula shelf

- spatially extensive, multi-year dFe and pFe distributions in WAP surface waters
- concurrent distributions of dMn, pMn, pAl and pTi to identify key Fe sources
- we document widespread low Fe conditions above the WAP shelf
- Fe enrichment was correlated with elevated proportions of meteoric water
- spatial and interannual variability in reductive sedimentary flux